FATIGUE EXPERIMENTS AND MODULUS DEGRADATION MODELING ON SHEET MOLDING COMPOUND

BY

TONY BOR-YIH TAI

B.S., University of Illinois, 1994

THESIS

Submitted in partial fulfillment of the requirements
for the degree of Master of Science in Mechanical Engineering
in the Graduate College of the
University of Illinois at Urbana-Champaign, 1996

Urbana, Illinois

Acknowledgment

This research was funded by the Fracture Control Program, Department of Mechanical and Industrial Engineering, University of Illinois at Champaign-Urbana. The materials were supplied by Navistar International Corporation and GenCorp.

I would like to express sincere appreciation to my advisor, Professor Huseyin Sehitoglu, for his guidance and encouragement in the last two years.

Special thanks are extended to Dr. Peter Kurath for conducting the experiments and helping me with the image analysis.

Most importantly, I dedicate all my accomplishments to my parents, Mr. and Mrs. Hung-cheng Tai. Thank you for the nurturing love and support, and the sacrifice that you have made for me.

Table of Contents

List of Tables

List of Figures

List of Symbols

D	Domain of an infinite body
Ω_1, Ω_2	Crack 1 and crack 2
f_1, f_2	Volume fractions of crack 1 and crack 2
C^0_{ijkl}	Elastic stiffness tensor of matrix
C^1_{ijkl}, C^2_{ijkl}	Elastic stiffness tensors of crack 1 and 2
'	Primed quantities referred to the local coordinate system
σ^0_{ij}	Applied stress
ε^0_{kl}	Applied strain
$\langle\sigma_{ij}\rangle_M$	Disturbance stress in the matrix due to average disturbance strains
σ^1_{ij}, σ^2_{ij}	Disturbance stresses due to crack 1 and 2
ε^1_{kl}, $\varepsilon^{2}_{kl}{}'$	Disturbance strains due to crack 1 and 2
$\bar{\varepsilon}_{kl}$	Average disturbance strain due to all cracks
ε^*_{kl}, $\varepsilon^{**}_{mn}{}'$	Eigenstrains due to crack 1 and 2
S^1_{klmn}, S^2_{klmn}	Eshelby tensors of crack 1 and 2
f_θ	Volume fraction of θth crack orientation
σ^θ_{ij}	Disturbance stress of θth crack orientation
$\varepsilon^{\theta*}_{ij}$	Disturbance strain of θth crack orientation
$C^{0}_{ijkl}{}^{-1}$	Compliance tensor of the matrix
$C^{c}_{ijkl}{}^{-1}$	Compliance tensor of the composite
σ_f	Fracture Strength
ε_f	Fracture Strain
R	Minimum stress over maximum stress
ΔS	Stress range
N_f	Final fatigue life

1. Introduction

Short fiber reinforced Sheet Molding Compound (SMC) has become one of the most important engineering materials in ground vehicle industry in recent years. Some of the advantages of using SMC include a high stiffness to weight ratio, superior strength, good corrosion resistance, and the ability to mold the material into complex shapes. In addition, the low manufacturing cost of SMC has prompted the industries to replace the traditional material such as sheet steel and metal alloys with SMC in many engineering applications, especially in the automotive industry.

Even though with the increasing applications using SMC, many mechanical properties are not well understood and need further research. One of the major concerns is the fatigue behavior of SMC. Specifically, the microstructural damages develop that lead to modulus degradations in long term applications and in turn determine the fatigue life of SMC.

The objectives of this research are to understand the fatigue behavior of the SMC composites and to develop a correlation between modulus, life, and the microstructural damages observed from fatigue experiments of SMC. There are six formulas of the SMC composites being studied, with each formula consisted of various compositions of the glass fiber, calcium carbonate filler, and resin matrix. The research consists of two major aspects. The first aspect includes conducting tensile and fatigue experiments on the SMC composites and performing image analysis on one of the SMC composites (FS4501, 45% glass fiber). The second aspect involves simulations of the modulus degradations in SMC composite, FS4501, using the Modulus Prediction Program developed in this study. This program calculates the degradation of elastic modulus as a function of volume fraction and orientation of cracks. The results have implications in estimating the residual life of

composites in service upon obtaining a photograph of the surface and predicting the modulus reduction.

Since the introduction of glass-fiber reinforced plastics for engineering applications, efforts devoted to research and developments of fiber-reinforced composites have been growing steadily. In particular, two researches are relevant and important to the development of this study. In 1987, Advani [1] studied fiber orientation for processing considerations and predicting mechanical properties. He used a tensor description to characterize and predict the orientation of fibers during flow. The orientation of the fibers plays the role of a structural state variable to establish a complete path from processing to properties of short fiber composites. In 1985, Chim [2] studied microscopic material damage and macroscopic property degradation in random short-fiber SMC composite subjected to cyclic tensile loading. He used the self-consistent mechanics analysis in conjunction with the probabilistic microcrack distribution functions introduced in the composite under fatigue loading. Both of these studies were examined during this research to better understand and forward a new model for fatigue damage in SMC.

2. Experiments

2.1 Materials

Sheet Molding Compound (SMC) consists of randomly distributed glass fibers and polyester resins. One of the preparation steps involves mixing of a resin paste which includes fillers, thickeners, initiators, lubricants, and pigments. The paste is then placed on a polyethylene carrier film in the SMC machine. A schematic of a standard SMC machine is shown in Figure 2.1. The glass fibers are chopped to 25.4 mm in length from continuous glass rovings and randomly dropped onto the resin paste. A second layer of carrier film with the resin paste is placed on top. The carrier films are then compacted and kneaded by going through a series of rollers. The kneading process removes most of the air pockets. Finally, the material is wound from the SMC machine into a large roll and stored for aging. The aging process allows the resin-fiber mixture to improve its viscosity in order to carry the reinforcement during flow.

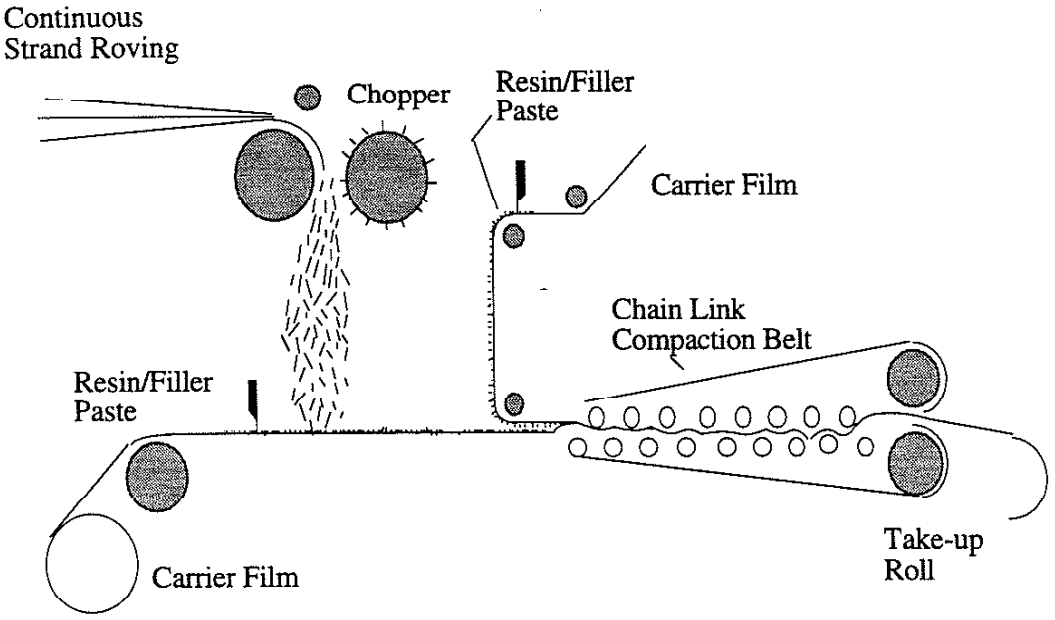

Figure 2.1 Standard SMC Machine

SMC parts are generally manufactured by the compression molding method. A schematic of the compression molding process is shown in Figure 2.2. A stack, or charge, of SMC is cut into the desired shape and dimension. The charge is then placed between a pair of hot dies. After the charge is properly positioned, the die set closes causing the charge to flow and fills the mold cavity. The high temperature in the mold causes exothermic polymerization in the SMC. Upon the completion of reaction, the mold is opened and the finished part is removed.

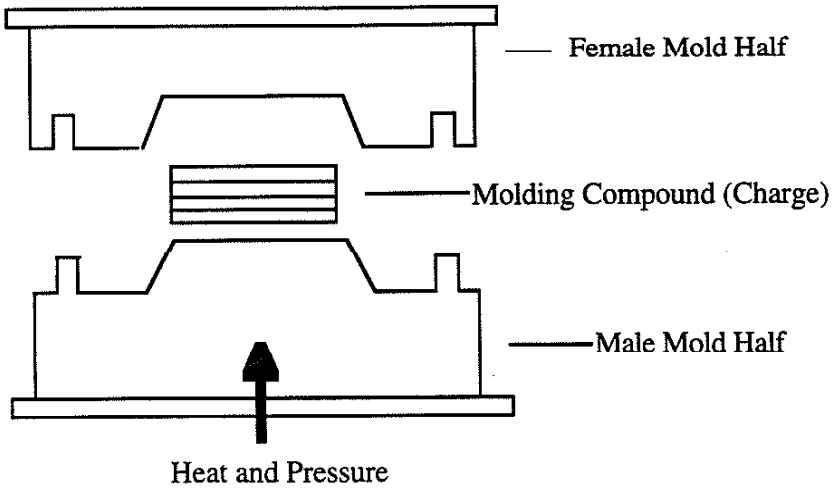

Figure 2.2 Schematic of Compression Molding Die for SMC Materials

The glass reinforcement fibers are added in various amount depending on the application of the SMC. In this research, there are six different formulas of sheet molding compound studied. The contents are listed in Table 2.1. Note these values given in the Table 2.1 are weight percentages, not volume fractions. The first three composites (FS3001, HF3502, and FS4501) were produced by Navistar International Transportation

Corporation. The last three composites (7160, Low Pressure 7525, and Quantum 8800) were produced by Gencorp Reinforced Plastics Division.

Formula	% Glass Fiber	% Filler	% Resin
FS3001	30	44	26
HF3502	35	40	25
FS4501	45	28	27
7160	27	-	-
Low Pressure 7525	27	-	-
Quantum 8800	62	-	-

Table 2.1 Formulation of all 6 compositions of Sheet Molding Compound

2.2 Experimental Techniques

There were two types of experiments performed on each of the six formulas of SMC. Monotonic tests were performed to establish the fracture strength and fracture strain of each composite. This information aided in choosing the stress levels for the fatigue experiments. The cyclic experiments were conducted to obtain the long term stress-strain behaviors of SMC. The information gathered from the fatigue tests was then used to study the effect of fatigue damage on the overall stiffness of SMC.

The specimens used in this study were cut from panels of SMC with dimensions of 300 mm by 300 mm and thicknesses of 2.5 mm. This thickness is typically larger than a molded part and was chosen to minimize buckling effects in compression. Each specimen had a total length of 85.5 mm and a total width of 25 mm. The gage length was 15 mm and the gage width was 19 mm. The geometry of these specimens is shown in Figure 2.3.

There were 27 specimens machined from each panel of SMC. To avoid edge effects, the material within 25.4 mm from all edges of the panels was not used for specimens.

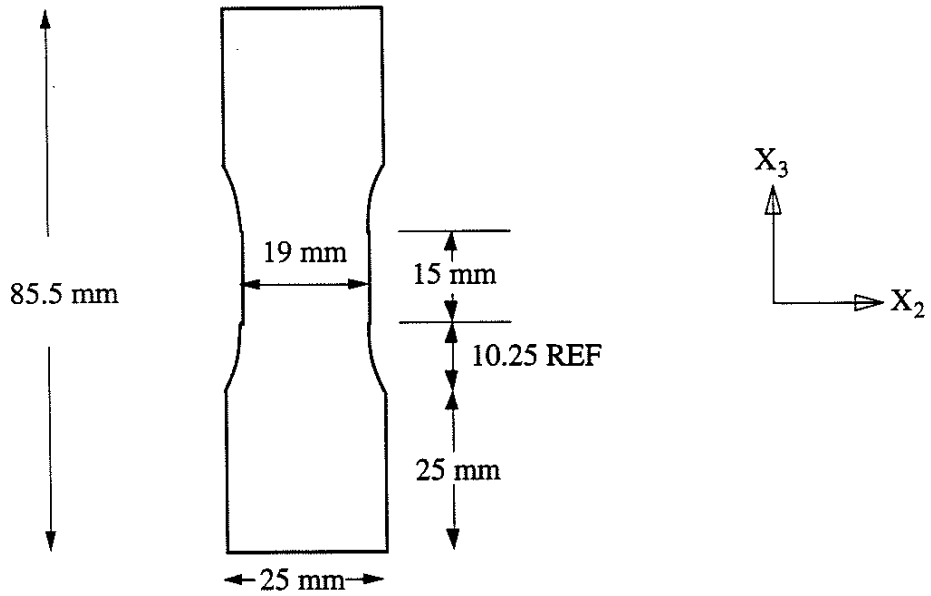

Figure 2.3 Schematic of SMC Specimen

There were a total of 9 monotonic tests and 129 cyclic tests completed. The list of experiments is shown in Appendix A. All experiments were conducted using Instron servohydraulic tensile testing systems. The monotonic tests were performed at room temperature by loading specimens in tension until fracture. The strains were measured by using clip-gage extensometers. The results were recorded using the Labview software on Macintosh computers.

The fatigue tests were also performed at room temperature using load controlled triangular waveform, and the frequencies were ranged between 2.5 and 5 Hz. Two different loading ratios were studied, $R \approx 0$ and $R = -1$. The value R represents the ratio of minimum stress over maximum stress of each test. For $R \approx 0$, in this study, the

minimum stress was not 0 MPa but 5 MPa. This allowed the specimens to be deformed in the tensile regime. Most of the fatigue experiments were cycled until failure. However, there were several interrupted tests performed on FS4501 in order to observe the fatigue damages at different stages (5%, 10%, and 25%) of the specimen life. Throughout each experiment, the loads, strains, and cycles of each specimen were stored by Labview software. From the information collected, Labview also generated the stress-strain plots.

2.3 Image Analysis

Image analysis was used to obtain damage information on SMC specimens, and the results were used to predict the modulus of the composites. The idea is to develop a onetime correlation between modulus, life, and the image obtained from the specimen. In this study, image analysis consisted of three major components. First, a Scanning Electron Microscope (SEM) was used to obtain photographs of fatigue damages from tested samples. Second, a scanning software was used to digitize the SEM photographs. This step was useful in converting normal photographs into digitized computer files to be analyzed later. Finally, the NIH Image Processing and Analysis Program was used to attain information such as crack dimensions, crack areas, and crack angles from digitized SEM photographs. These data sets were then used to predict the modulus of the tested SMC composites using a micro-mechanical analysis.

In order to obtain photographs of Sheet Molding Compound using the SEM, the tested specimen had to be properly prepared. First, a sample of approximately 19 mm by 7 mm was cut from the gage sections of the tested specimen. Due to the fact that there was a layer of polyethylene on the exterior of the specimen hindering the visibility of the damaged sample, the sample was cut again through the thickness direction. The next step was polishing the cut surface by using Buehler 6 μm polisher followed by a Buehler 0.05 μm polisher. The sample was then placed in an ultrasonic cleaner for five minutes to shake off any dirt and particles that might have deposited on the sample surfaces. SMC is a non

conductive polymer composite, therefore, proper curing and sputtering was necessary in order to observe the material under the SEM. The sample was attached on a circular Hitachi mount using a lead paste, and the curing process took approximately 18 to 24 hours. This process ensured proper spreading of gold during the sputtering process. After curing, the sample was ready for the last step of preparation - sputtering. In this study, gold was used for sputtering SMC. The cured sample along with the Hitachi mount were placed in the vacuum chamber of a sputter. By following the sputtering procedures and setting the timer and current to 60 seconds and 30 mili-amp, respectively, the sample was ready to be placed into the SEM.

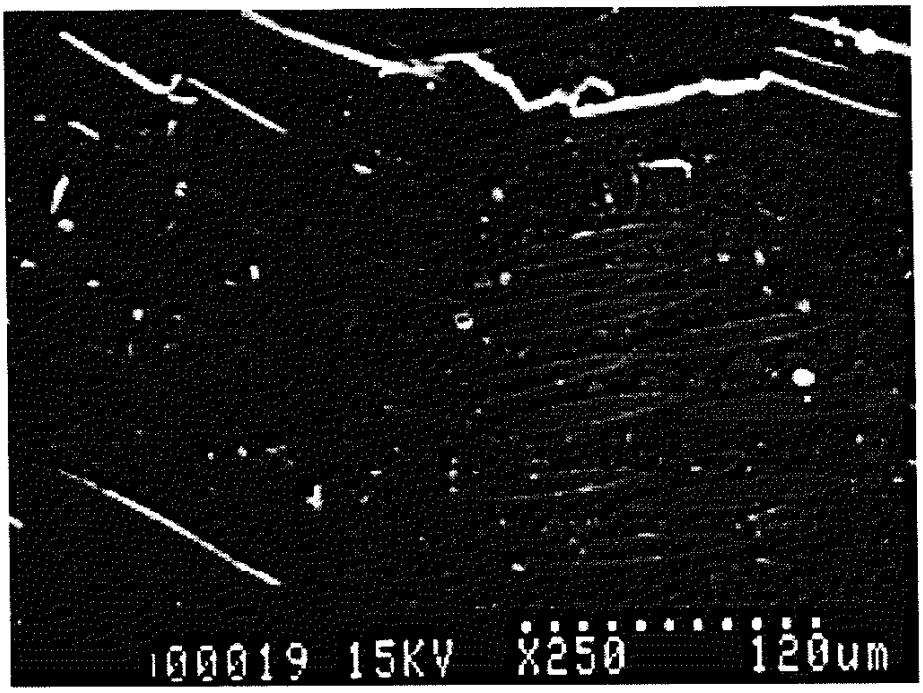

Figure 2.4 A Digitized Scanning Electron Microscope Photograph of SMC (FS4501)

The Scanning Electron Microscope used in this research was the Hitachi S-570 SEM with acceleration voltage set at 15 kilo-volts and the working distance kept at 28 mm.

The Polaroid Instant Sheet Film with a speed of 55 was used to obtain the SEM photographs. The Hitachi S-570 SEM had the capability of delivering high resolution photographs at very high magnificaions, but in this study, each SEM photograph was composed of 6 individual photographs that were magnified at 250 times. An example of SEM photograph is shown in Figure 2.4. The light gray areas with long strand shapes are the glass fibers. The other light gray areas with polygon shapes are the calcium carbonate fillers. The dark gray background is the polymer matrix. Finally, the white areas are the fatigue cracks. Note that fatigue cracks are visible at fiber-matrix interfaces and filler-matrix interfaces.

In order to attain information from the SEM photographs, the photographs had to be digitized. Ofoto scanning software was used to digitize the SEM photographs. By placing the photographs on the scanner, Ofoto went through a series of scanning processes and saved the digitized photographs as computer files.

NIH Image Processing and Analysis Program was used to obtain information from digitized SEM photographs. There were four areas of interest in determining the degraded modulus: crack area fraction, crack angle, crack length, and crack width. The first step in using NIH Image was to set the appropriate scale. This was achieved by choosing the 'select lines' option in Tools from the screen, highlighting the scale ruler from the digitized SEM photographs, and then selecting the 'scale' option in the Analyze menu. All the SEM photographs were magnified 250 times and had the same scale ruler of 120 μm. Upon completion of this step, all the measurement would have units in μm. The second step was determining the overall area of the study. This was done by choosing the 'rectangular select regions' option in Tools from the screen, high lighting the area of study, and then selecting the 'measure' option in the Analyze menu. The third step was very similar to the second step; instead of selecting the overall area, crack areas were selected one at a time by tracing the perimeter of the cracks using appropriate 'select regions' option. The fourth step was determining the angle of inclination of cracks. This process was done by

choosing the 'measure angle' option in Tools from the screen, drawing two segments of a line, one segment being parallel to the length of the crack, and one segment being horizontal. The fifth step was measuring the length of the cracks. This was done by choosing the 'select lines' option in Tools from the screen, high lighting the length of the crack, and then selecting the 'measure' option in the Analyze menu. The sixth step was performed in the same manner as the fifth step with one difference, instead of selecting the length of the crack the width of the crack was selected. Step 3 through 6 were repeated for all cracks within the area of interest. The results were tabulated and could be shown by choosing the 'show results' option in the Analyze menu. Upon completion of measurements, the results were tabulated and sorted using Microsoft Excel software. The table was sorted in the order of area fraction, crack angle, crack length, and crack width.

3. Theoretical Development

3.1 Background

The fatigue life of SMC is largely determined by the amount of the microstructural damages accumulated throughout the life. The microstructural damages include matrix cracking, fiber-matrix debonding, and filler-matrix debonding. When the material is subjected to tensile loadings, the existing cracks grow, in addition, new cracks initiate. As the volume fraction of the microstructural damage increases, the modulus of the SMC composites decreases. The modulus degradation is determined by the volume fraction and the orientation of the cracks. By understanding how to model the fatigue cracks, the modulus can be determined for any fatigue damaged SMC composites.

In this research, the fatigue cracks are modeled as ellipsoidal inclusions in the composite. Eshelby first pointed out that the stress disturbance in an applied stress due to the presence of an inhomogeneity can be simulated by an eigenstress caused by an inclusion when the eigenstrain is chosen properly [3]. The modulus of the composite with ellipsoidal inclusion can be easily solved once the corresponding eigenstrain is computed by Eshelby's equivalent inclusion method [4]. However, Eshelby's equivalent inclusion method does not take into account the interaction effect of the inclusions when the volume fraction of inclusion becomes large. Mori and Tanaka [5] modified Eshelby's method which accounts for the interactions among the inclusions. Mori and Tanaka applied their work to only one type of inclusion in a composite. In recent years, Taya and Chou [6] extended Mori-Tanaka's analysis to include two types of inclusions and solved for the modulus of a three-phase composite.

The theoretical development of this research is based on Eshelby's equivalent inclusion method [4] and Mori-Tanaka's analysis [5]. The formulation follows Taya and Chou's work [6] closely with modifications in three areas. First, the inhomogenieties are

the fatigue cracks instead of fibers and fillers. Second, the following formulation is not limited in number of inclusion types. Last, the equations are developed to include various orientations of cracks.

3.2 Formulation

Consider an infinite elastic body which contains two orientations of cracks and subject to the applied stress σ_{ij}^{0}. A schematic of the elastic body is shown in Figure 3.1(a). Let the domain of the infinite body be denoted by D, and the cracks be denoted by Ω_1 and Ω_2. Therefore, the domain of the matrix is $D-\Omega_1-\Omega_2$. The elastic stiffness tensors of the matrix, crack Ω_1 and Ω_2 are denoted by C_{ijkl}^{0}, C_{ijkl}^{1}, and C_{ijkl}^{2}, respectively. The volume fraction of Ω_1 and Ω_2 are denoted by f_1 and f_2, respectively.

Following Mori and Tanaka [5], under the applied stress σ_{ij}^{0}, the average of the total stress in the matrix is given by $\sigma_{ij}^{0}+\langle\sigma_{ij}\rangle_M$, where

$$\langle\sigma_{ij}\rangle_M = C_{ijkl}^{0}\,\bar{\varepsilon}_{kl} \tag{1}$$

Here, $\langle\ \rangle$ denotes the volume average of a quantity and $\bar{\varepsilon}_{kl}$ stands for the average disturbance of strain due to the presence of crack Ω_1 and Ω_2.

Introducing a single crack, Ω_1, into the infinite elastic body with the orientation defined by θ, see Figure 3.1(b). In Eshelby's equivalent inclusion method [4], eigenstrain ε_{kl}^{*} is used to simulate the strain disturbance which occupies the space Ω_1. By applying the equivalent inclusion method in composite body D, yields

$$\begin{aligned}\sigma_{ij}^{0}+\sigma_{ij}^{1} &= C_{ijkl}^{0}\left(\varepsilon_{kl}^{0}+\bar{\varepsilon}_{kl}+\varepsilon_{kl}^{1}-\varepsilon_{kl}^{*}\right)\\ &= C_{ijkl}^{1}\left(\varepsilon_{kl}^{0}+\bar{\varepsilon}_{kl}+\varepsilon_{kl}^{1}\right)\end{aligned} \tag{2}$$

where σ_{ij}^{1} and ε_{kl}^{1} are the disturbance of the stress and strain due to this single crack,

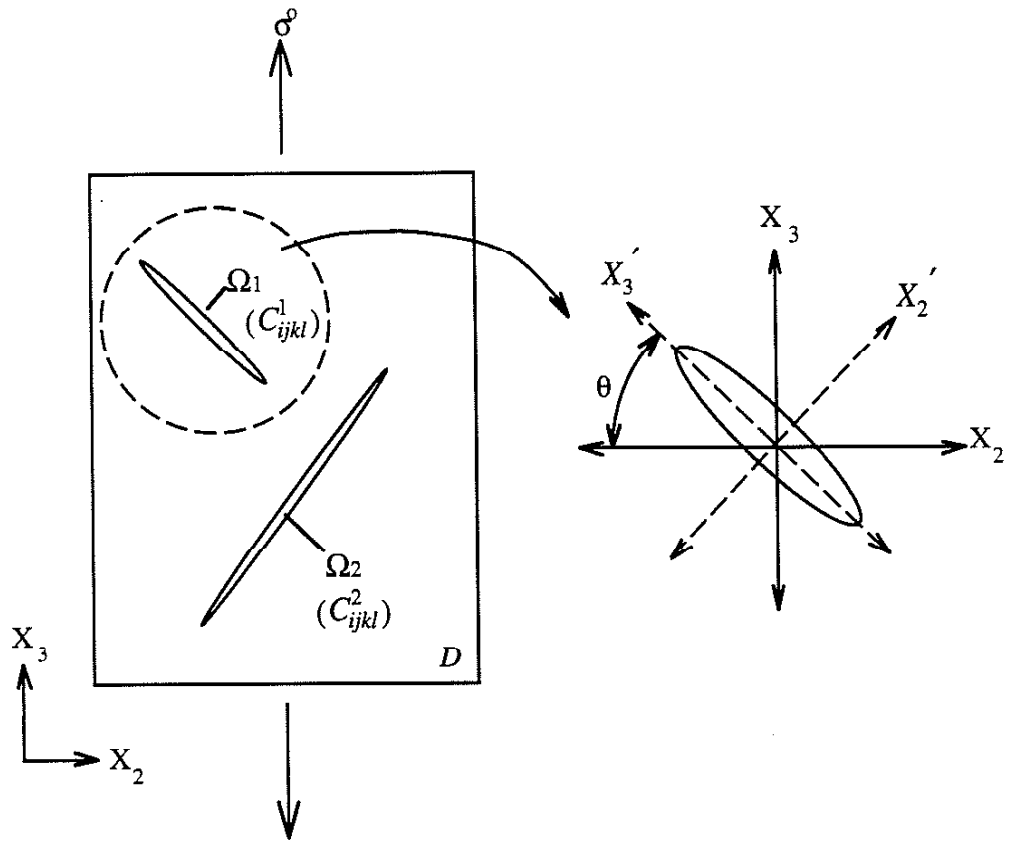

(a) (b)

Figure 3.1 (a)Calculation model of an infinite elastic body D with crack Ω_1 and Ω_2. (b)Crack orientation of crack Ω_1 .

respectively. It is more convenient to use the local coordinate system x_1', x_2', and x_3', where the x_3' axis is the fiber direction. Therefore, the equivalent inclusion method becomes

$$\overset{\circ}{\sigma}{}^{0\prime}_{ij} + \sigma^{1\prime}_{ij} = C^{0}_{ijkl}\left(\varepsilon^{0\prime}_{kl} + \bar{\varepsilon}_{kl}{}' + \varepsilon^{1\prime}_{kl} - \varepsilon^{*\prime}_{kl} \right)$$

$$= C^1_{ijkl}\left(\varepsilon^{0}_{kl}{}' + \bar{\varepsilon}_{kl}{}' + \varepsilon^{1}_{kl}{}' \right) \tag{3}$$

where $\sigma^1_{ij}{}'$ is the disturbances of stress due to this single crack, $\varepsilon^1_{kl}{}'$ is the strain due to this single crack, and $\varepsilon^*_{kl}{}'$ is the eigenstrain, or transformation strain, which has nonvanishing components in Ω_1, but becomes zero outside Ω_1. The prime represents tensorial quantities referred to the local coordinate system $x_1{}'$, $x_2{}'$, and $x_3{}'$. According to Hooke's law,

$$\sigma^{0}_{ij}{}' = C^{0}_{ijkl}\,\varepsilon^{0}_{kl}{}' \tag{4}$$

Using eqn. (4), eqn (3) yields

$$\sigma^1_{ij}{}' = C^0_{ijkl}\left(\bar{\varepsilon}_{kl}{}' + \varepsilon^1_{kl}{}' - \varepsilon^*_{kl}{}' \right) \tag{5}$$

Following Eshelby [4],

$$\varepsilon^1_{kl}{}' = S^1_{klmn}\varepsilon^*_{mn}{}' \qquad \text{in } \Omega_1 \tag{6}$$

where S^1_{klmn} is the Eshelby's tensor (see [4] for details) which depends on C^0_{ijkl} and the geometry of Ω_1.

Next we add another single crack, Ω_2, with a different crack orientation angle to this composite system D. Following the previous formulation,

$$\begin{aligned} \sigma^{0}_{ij}{}' + \sigma^{2}_{ij}{}' &= C^{0}_{ijkl}\left(\varepsilon^{0}_{kl}{}' + \bar{\varepsilon}_{kl}{}' + \varepsilon^{2}_{kl}{}' - \varepsilon^{**}_{kl}{}' \right) \\ &= C^{2}_{ijkl}\left(\varepsilon^{0}_{kl}{}' + \bar{\varepsilon}_{kl}{}' + \varepsilon^{2}_{kl}{}' \right) \end{aligned} \tag{7}$$

using eqn (4), eqn (7) yields

$$\sigma_{ij}^{2\prime} = C_{ijkl}^{o}\left(\bar{\varepsilon}_{kl}^{\prime} + \varepsilon_{kl}^{2\prime} - \varepsilon_{kl}^{*\prime}\right) \tag{8}$$

Also, $\varepsilon_{kl}^{2\prime}$ is related to $\varepsilon_{mn}^{**\prime}$ by

$$\varepsilon_{kl}^{2\prime} = S_{klmn}^{2}\varepsilon_{mn}^{**\prime} \qquad \text{in } \Omega_2 \tag{9}$$

where $\varepsilon_{mn}^{**\prime}$ is the eigenstrain due to crack Ω_2, and S_{klmn}^{2} depends on C_{ijkl}^{o} and the geometry of Ω_2.

The local coordinate system can be transformed to the global coordinate system by using the coordinate transformation rule. By using the vector notation,

$$\begin{aligned}
\varepsilon_{ij}^{o\prime} &= (-\nu, \sin^2\theta - \nu\cos^2\theta, -\nu\sin^2\theta + \cos^2\theta, \\
&\qquad 0, 0, (1+\nu)\sin\theta\cos\theta)^t \frac{\sigma^o}{E_o} \\
\bar{\varepsilon}_{ij}^{\prime} &= (\bar{\varepsilon}_{22}, \bar{\varepsilon}_{33}\sin^2\theta + \bar{\varepsilon}_{22}\cos^2\theta, \bar{\varepsilon}_{22}\sin^2\theta + \bar{\varepsilon}_{33}\cos^2\theta, \\
&\qquad 0, 0, (\bar{\varepsilon}_{33} - \bar{\varepsilon}_{22})\sin\theta\cos\theta)^t
\end{aligned} \tag{10}$$

where t denotes the transpose.

Since the disturbed stress σ_{ij} must satisfy $\int_D \sigma_{ij} dV = 0$, then

$$(1 - f_1 - f_2)\langle\sigma_{ij}\rangle_M + f_1\left(\sigma_{ij}^{1}\right) + f_2\left(\sigma_{ij}^{2}\right) = 0 \tag{11}$$

where $\langle\ \rangle$ denotes the volume averaged quantity. The above formulation is written for a composite body with two crack orientations. It should be noted that the formulation above is applicable to a composite body with unlimited number of crack orientations. Eqn (11) has the form of

$$\left(1-\sum_{\theta} f_{\theta}\right)\left\langle \sigma_{ij}\right\rangle_{M}+\sum_{\theta} f_{\theta}\left(\sigma_{ij}^{\theta}\right)=0 \qquad (12)$$

where f_{θ} represents the volume fraction and σ_{ij}^{θ} denotes the disturbance stress of θth crack orientation.

To solve for the overall modulus of the composite, the first step is to eliminate $\varepsilon_{ij}^{1}{}'$ and $\varepsilon_{ij}^{2}{}'$ through eqns (6) and (9). Second, by using vector transformation in eqn (10), the only unknowns are ε_{ij}^{*}, ε_{ij}^{**}, and $\bar{\varepsilon}_{ij}$. Third, by using eqns (3), (7), and (11), ε_{ij}^{*} and ε_{ij}^{**} are solved in terms of $\bar{\varepsilon}_{ij}$. Finally, the overall modulus of the composite is computed by using the equivalence of the strain energies

$$\frac{1}{2}C_{ijkl}^{c\ -1}\sigma_{ij}^{0}\sigma_{kl}^{0}=\frac{1}{2}C_{ijkl}^{0\ -1}\sigma_{ij}^{0}\sigma_{kl}^{0}+\frac{1}{2}f_{1}\sigma_{ij}^{0}\varepsilon_{ij}^{*}+\frac{1}{2}f_{2}\sigma_{ij}^{0}\varepsilon_{ij}^{**} \qquad (13)$$

or,

$$\frac{1}{2}C_{ijkl}^{c\ -1}\sigma_{ij}^{0}\sigma_{kl}^{0}=\frac{1}{2}C_{ijkl}^{0\ -1}\sigma_{ij}^{0}\sigma_{kl}^{0}+\sum_{\theta}\frac{1}{2}f_{\theta}\sigma_{ij}^{0}\varepsilon_{ij}^{\theta*} \qquad (14)$$

where $C_{ijkl}^{0\ -1}$ and $C_{ijkl}^{c\ -1}$ are the compliances of the matrix and the composite, respectively, and $\varepsilon_{ij}^{\theta*}$ denotes the transformation strain of θth crack orientation. The details of the derivation of eqn (13) are given in [6].

3.3 Implementation of the Model

The Modulus Prediction Program is written based on the above formulations. Given that the applied stress is σ_{33}^{0}, σ_{11}^{0} equals to zero, and since SMC is a planar isotropic material and the cracks are assumed to be ellipsoidal inclusions, the only non-vanishing terms are ε_{ij}^{*}, ε_{ij}^{**}, and $\bar{\varepsilon}_{ij}$ where ij = 22, 33, and 23. The tensorial eqn (3) for inclusion, Ω_1, is simplified to

$$A\left(\varepsilon_{22}^{*}{}'\right)+B\left(\varepsilon_{33}^{*}{}'\right)=C\left(\varepsilon_{22}^{0}{}'+\bar{\varepsilon}_{22}{}'\right)+D\left(\varepsilon_{33}^{0}{}'+\bar{\varepsilon}_{33}{}'\right) \tag{15}$$

$$E\left(\varepsilon_{22}^{*}{}'\right)+F\left(\varepsilon_{33}^{*}{}'\right)=G\left(\varepsilon_{22}^{0}{}'+\bar{\varepsilon}_{22}{}'\right)+H\left(\varepsilon_{33}^{0}{}'+\bar{\varepsilon}_{33}{}'\right) \tag{16}$$

$$\left(\varepsilon_{23}^{*}{}'\right)=J\left(\varepsilon_{23}^{0}{}'+\bar{\varepsilon}_{23}{}'\right) \tag{17}$$

where

$$\begin{aligned}
A &= C_{2211}^{0}S_{1122}^{*}+C_{2222}^{0}S_{2222}^{*}+C_{2233}^{0}S_{3322}^{*}-C_{2222}^{0}-C_{2222}^{*}\\
B &= C_{2211}^{0}S_{1133}^{*}+C_{2222}^{0}S_{2233}^{*}+C_{2233}^{0}S_{3333}^{*}-C_{2233}^{0}-C_{2233}^{*}\\
C &= C_{2222}^{*}-C_{2222}^{0}\\
D &= C_{2233}^{*}-C_{2233}^{0}\\
E &= C_{3311}^{0}S_{1122}^{*}+C_{3322}^{0}S_{2222}^{*}+C_{3333}^{0}S_{3322}^{*}-C_{3322}^{0}-C_{3322}^{*}\\
F &= C_{3311}^{0}S_{1133}^{*}+C_{3322}^{0}S_{2233}^{*}+C_{3333}^{0}S_{3333}^{*}-C_{3333}^{0}-C_{3333}^{*}\\
G &= C_{3322}^{*}-C_{3322}^{0}\\
H &= C_{3333}^{*}-C_{3333}^{0}\\
J &= \left(C_{2323}^{*}-C_{2323}^{0}\right)\Big/\left(C_{2323}^{0}S_{2323}^{*}+C_{2323}^{0}-C_{2323}^{*}\right)
\end{aligned} \tag{18}$$

The S^{*}, C^{0}, and C^{*} terms in eqn (18) are known. $\varepsilon_{22}^{*}{}'$, and $\varepsilon_{33}^{*}{}'$ are solved as following,

$$\varepsilon_{22}^{*\prime} = \frac{(ACF - ABG)}{(A^2F - AEB)}\left(\varepsilon_{22}^{o\prime} + \bar{\varepsilon}_{22}^{\prime}\right) + \frac{(ADF - ABH)}{(A^2F - AEB)}\left(\varepsilon_{33}^{o\prime} + \bar{\varepsilon}_{33}^{\prime}\right) \tag{19}$$

$$\varepsilon_{33}^{*\prime} = \frac{(AG - EC)}{(AF - EB)}\left(\varepsilon_{22}^{o\prime} + \bar{\varepsilon}_{22}^{\prime}\right) + \frac{(AH - DE)}{(AF - EB)}\left(\varepsilon_{33}^{o\prime} + \bar{\varepsilon}_{33}^{\prime}\right) \tag{20}$$

Substituting eqn (10), from local to global transformation of strains, into eqn (17), (19), and (20), $\varepsilon_{22}^{*\prime}$, $\varepsilon_{33}^{*\prime}$, and $\varepsilon_{23}^{*\prime}$ are expressed in terms of $\bar{\varepsilon}_{22}$ and $\bar{\varepsilon}_{33}$.

Eqn (7) for inclusion, Ω_2, is also simplified as above, but instead of $\varepsilon_{22}^{*\prime}$, $\varepsilon_{33}^{*\prime}$, and $\varepsilon_{23}^{*\prime}$, they are replaced by $\varepsilon_{22}^{**\prime}$, $\varepsilon_{33}^{**\prime}$, and $\varepsilon_{23}^{**\prime}$, respectively. Again substituting eqn (10) into eqn (17), (19), and (20), $\varepsilon_{22}^{**\prime}$, $\varepsilon_{33}^{**\prime}$, and $\varepsilon_{23}^{**\prime}$ are expressed in terms of $\bar{\varepsilon}_{22}$ and $\bar{\varepsilon}_{33}$.

The tensorial eqn (11) is simplified to two equations with ij = 22 and 33.

$$\begin{aligned}(1 - f_1 - f_2)\langle\sigma_{22}\rangle_M + f_1\left(\sigma_{22}^1\right) + f_2\left(\sigma_{22}^2\right) &= 0\\ (1 - f_1 - f_2)\langle\sigma_{33}\rangle_M + f_1\left(\sigma_{33}^1\right) + f_2\left(\sigma_{33}^2\right) &= 0\end{aligned} \tag{21}$$

where σ_{22}^1, σ_{22}^2, σ_{33}^1 and σ_{33}^2 are given as

$$\begin{aligned}\sigma_{ij}^1 &= C_{ijkl}^o\left(\bar{\varepsilon}_{kl} + \varepsilon_{kl}^1 - \varepsilon_{kl}^*\right)\\ \sigma_{ij}^2 &= C_{ijkl}^o\left(\bar{\varepsilon}_{kl} + \varepsilon_{kl}^2 - \varepsilon_{kl}^{**}\right)\end{aligned} \tag{22}$$

, and where $\langle\sigma_{22}\rangle_M$ and $\langle\sigma_{33}\rangle_M$ are the stresses in the matrix due to the average disturbance strains and are defined in eqn (1). σ_{22}^1, σ_{22}^2, σ_{33}^1 and σ_{33}^2 are the disturbance stresses due to the inclusions in direction 2 and 3. Eqn (22) is rewritten using eqn (6) and (9) as

$$\sigma_{ij}^{1} = C_{ijkl}^{o}\left(\bar{\varepsilon}_{kl} + S_{klmn}^{1}\varepsilon_{mn}^{*} - \varepsilon_{kl}^{*}\right)$$
$$\sigma_{ij}^{2} = C_{ijkl}^{o}\left(\bar{\varepsilon}_{kl} + S_{klmn}^{2}\varepsilon_{mn}^{**} - \varepsilon_{kl}^{**}\right) \qquad (23)$$

To solve for the eigenstrains, ε_{33}^{*} and ε_{33}^{**}, first eqn (21) is rewritten in terms of $\bar{\varepsilon}_{22}$ and $\bar{\varepsilon}_{33}$ by substituting eqn (1) and (23) (where the disturbance stresses, σ_{ij}^{1} and σ_{ij}^{2}, are found by substituting the transformed $\varepsilon_{22}^{*\prime}$, $\varepsilon_{33}^{*\prime}$, $\varepsilon_{23}^{*\prime}$, $\varepsilon_{22}^{**\prime}$, $\varepsilon_{33}^{**\prime}$, and $\varepsilon_{23}^{**\prime}$ from local to global coordinate system). Now $\bar{\varepsilon}_{22}$ and $\bar{\varepsilon}_{33}$ in eqn (21) can be solved with two equations and two unknowns. By substituting $\bar{\varepsilon}_{22}$ and $\bar{\varepsilon}_{33}$ back into eqn (17), (19), (20), and using coordinate transformation, ε_{33}^{*} and ε_{33}^{**} are solved. Once ε_{33}^{*} and ε_{33}^{**} are solved, eqn (13) is used to solve for the modulus in the loading direction. Specializing for the uniaxial stress, σ_{33}^{o}, case we obtain,

$$\frac{1}{2}{C_{3333}^{c}}^{-1}\sigma_{33}^{o}\sigma_{33}^{o} = \frac{1}{2}{C_{3333}^{o}}^{-1}\sigma_{33}^{o}\sigma_{33}^{o} + \frac{1}{2}f_1\sigma_{33}^{o}\varepsilon_{33}^{*} + \frac{1}{2}f_2\sigma_{33}^{o}\varepsilon_{33}^{**} \qquad (24)$$

Since ε_{33}^{*} and ε_{33}^{**} are known, ${C_{3333}^{c}}^{-1}$ (inverse longitudinal modulus) is determined.

The calculation procedure for eigenstrains is the same for all inclusions in this case, therefore, there is no limit to the number of inclusions in the Modulus Prediction Program. The parameter value of the program can be set at a large value to accommodate a large number of inclusions (cracks).

The way the program is used in this study is as follows. After obtaining a picture of the damaged surface, the photograph is digitized and the volume fractions of cracks at specific orientations, f_θ, are established. Then, equation (14) is specialized for the case of uniaxial loading, i.e.. $\sigma_{ij}^{o} = \sigma_{33}$. The solution requires specification of properties in the absence of cracks. These properties were measured for the virgin material, E_{33}^{o}, E_{22}^{o}, ν_{23}^{o}, and ν_{31}^{o}. It was found that only E_{33}^{o} was the most important parameter. In the simulation, the cracks were treated as the material with very small modulus (for the crack,

$E_{33}^{*} = E_{22}^{*} \rightarrow 0.1$). The program calculates the stiffness tensor using the material properties. Along with the microstructural damage information, the Modulus Prediction Program computes the eigenstrains and in turn solves for the longitudinal modulus. The computer program is given in Appendix C.

4. Experimental Results

4.1 Tensile Test Results

There was a total of 9 monotonic tensile experiments performed during the course of research (tabulated in Appendix A). An example of a stress vs. strain plot for one of the SMC composites (FS3001), obtained from the tensile experiments, is shown in Figure 4.1. Notice the slopes of the stress-strain curve changed continuously and started at very early stages of the experiment. This indicated the initiation of the microstructural damages and continuing accumulation of damages under the first loading. In addition, the composite was brittle with fracture strain of 0.013. The shapes of all six composites of SMC were very similar (see Appendix B1). However, the fracture strength varied greatly. The results of the initial modulus, fracture strength, and fracture strains are listed in Table 4.1. Both the modulus and the strength of the composites increased with increasing percentages of glass fiber. The initial modulus of the SMC composites ranged from 8,578 MPa (LP7525) to 17,601 MPa (Quantum 8800). Quantum 8800 with a composition of 62% glass fiber

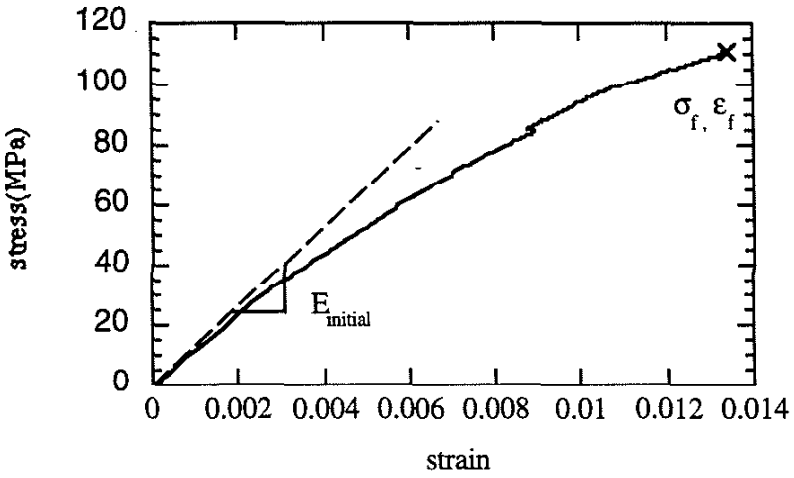

Figure 4.1 Tensile experiment result of FS3001, stress vs. strain.

had the highest fracture strength of 270 MPa. The LP7525 with a composition of 27% glass fiber had the lowest fracture strength of 84 MPa. The fracture strains ranged from approximately 0.013 to 0.024. The monotonic experiment results aided in choosing the stress levels for the fatigue experiments.

Materials	$E_{initial}$ (MPa)	σ_f (MPa)	ε_f
FS3001	11,656	110	0.013
HF3502	14,553	130	0.014
FS4501	16,830	137	0.024
7160	11,218	89	0.015
LP7525	8,578	84	0.020
Quantum 8800	17,601	270	0.021

σ_f = Fracture Strength
ε_f = Fracture Strain

Table 4.1 Tensile Properties of Sheet Molding Compound

4.2 Fatigue Results

4.2.1 Stress-strain Behavior in Fatigue

Fatigue tests were conducted on all six SMC composites under R=-1 and R≈0 loading conditions. All experiments were performed under stress controlled conditions, and there was a total of 129 cyclic experiments performed on the SMC (tabulated in Appendix A). The examples of stress vs. strain plots obtained from the R=-1 and R≈0 loading experiments are shown in Figure 4.2 and 4.3, respectively. Figure 4.2 is obtained from the cyclic experiment on FS3001 with the maximum loading stress of +50 MPa and the minimum loading stress of -50 MPa (R=-1 loading). Figure 4.3 is obtained from the

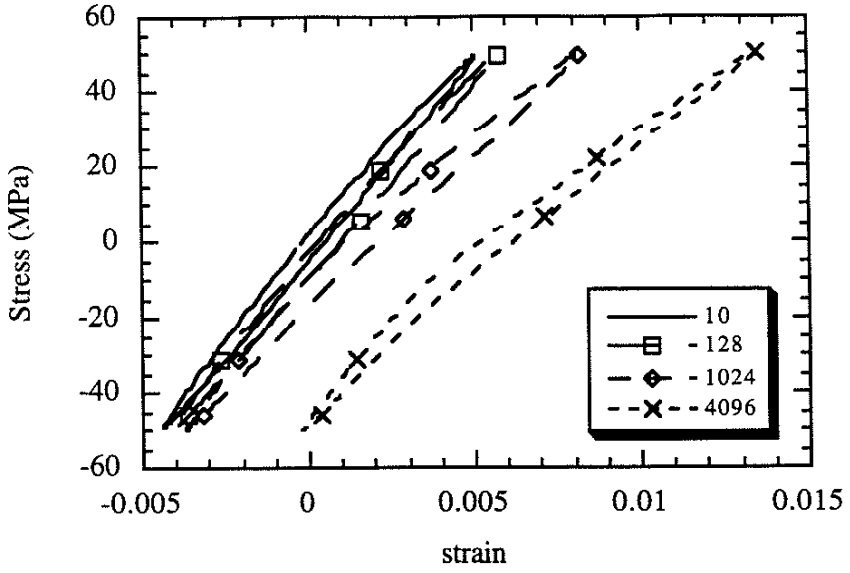

Figure 4.2 Stress-strain behavior of FS3001 under R=-1, ΔS=100 MPa loading (Frequency=3Hz, N_f=7,319).

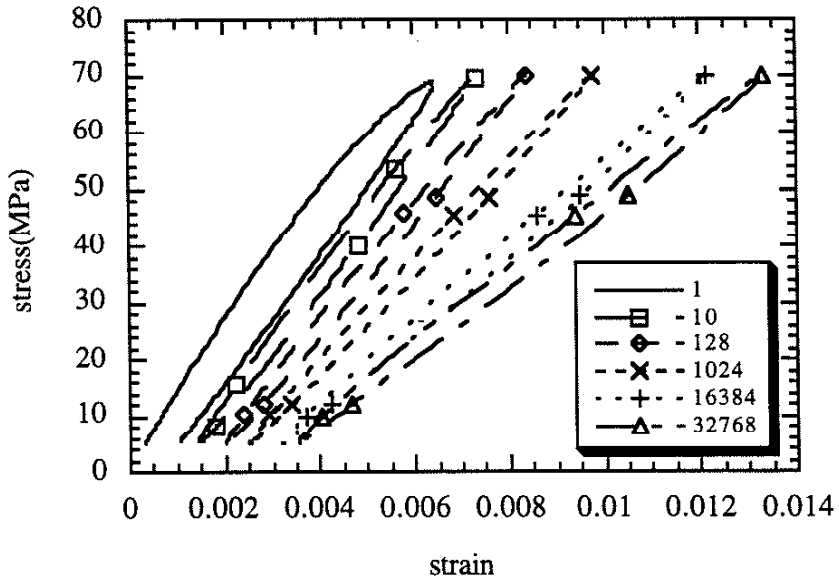

Figure 4.3 Stress-strain behavior of FS3001 under R≈0, ΔS=65 MPa loading (Frequency=3Hz, Nf=47,306)

cyclic experiment on FS3001 with the maximum loading stress of 70 MPa and the minimum loading stress of 5 MPa (R≈0 loading). The examples of stress vs. strain plots, obtained from the fatigue experiments, for the other SMC composites are shown in Appendix B2.

There were a few distinct characterizations observed from Figure 4.2 and 4.3. First of all, the slopes of the hysteresis loops decreased with increased number of cycles. This indicated the modulus reduction with increased number of cycles. Second, the modulus degradation occurred not only as a function of fatigue cycles, but also at different locations of the hysteresis loop within one cycle. Figure 4.4 is a plot of modulus vs. strain for cycle #1 of FS3001, and Figure 4.5 illustrates how the modulus value was obtained. The modulus measurements were performed by manual computations; the process involved computing the differences of stresses and strains of near by data points of the interested strain location and dividing the differences of stresses and strains to obtain the modulus

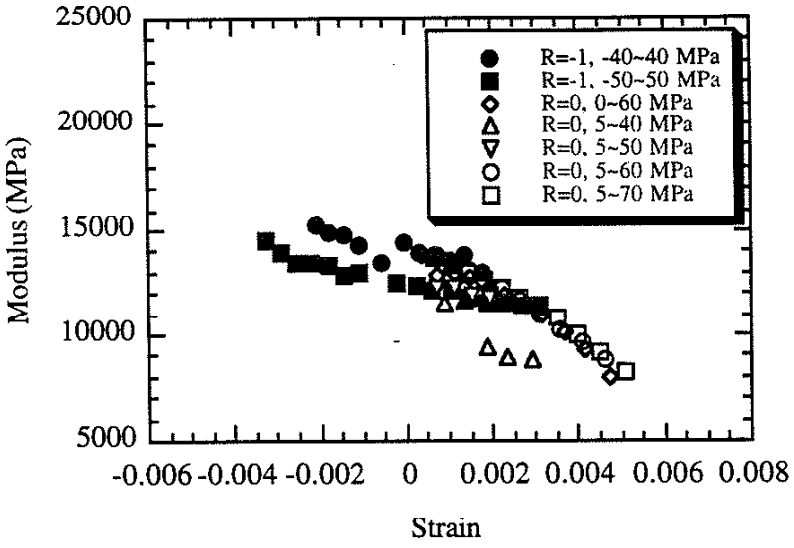

Figure 4.4 Modulus degradation of cycle #1 for FS3001, modulus vs. strain.

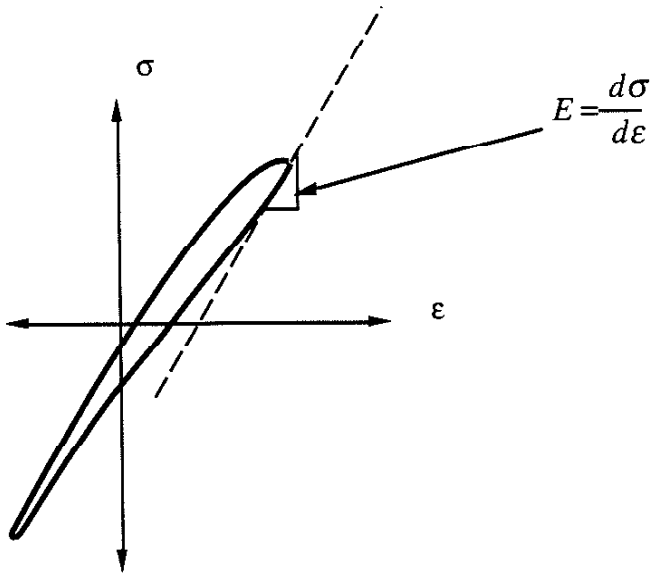

Figure 4.5 Illustration of modulus measurement

value. There were several experiments tabulated in Figure 4.4. From Figure 4.4, all experiments followed a general modulus decreasing trend ranging from 15,000 MPa to 8,000 MPa. With the exception of 5-40 MPa experiment, the modulus degradations were fairly consistent. Third, there was considerable ratchetting in the experiments shown in both Figure 4.2 and 4.3. However, there was less ratchetting in the other composites. The three characterizations showed the microstructural damages initiated at early stages of life and continued growth and accumulation of the damages throughout the fatigue life resulting in modulus degradations and ratchetting of the specimen.

4.2.2 Fatigue Life Results

The maximum loading stress vs. fatigue life of all six SMC composites were plotted in Figure 4.6 through Figure 4.9. Summaries of the results are tabulated in Appendix A. The arrows in the figures represented run-out experiments (specimen did not fail).

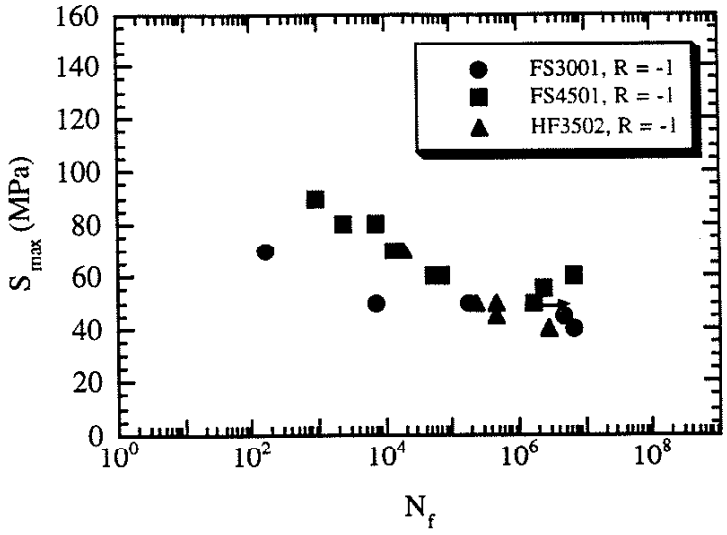

Figure 4.6 The maximum loading stress vs. fatigue life, R = -1 loading for FS3001, HF3502, FS4501.

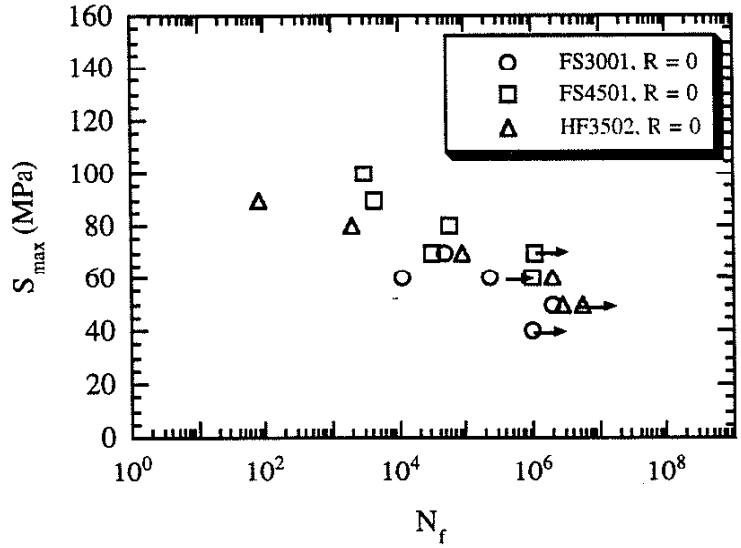

Figure 4.7 The maximum loading stress vs. fatigue life, R ≈ 0 loading for FS3001, HF3502, FS4501.

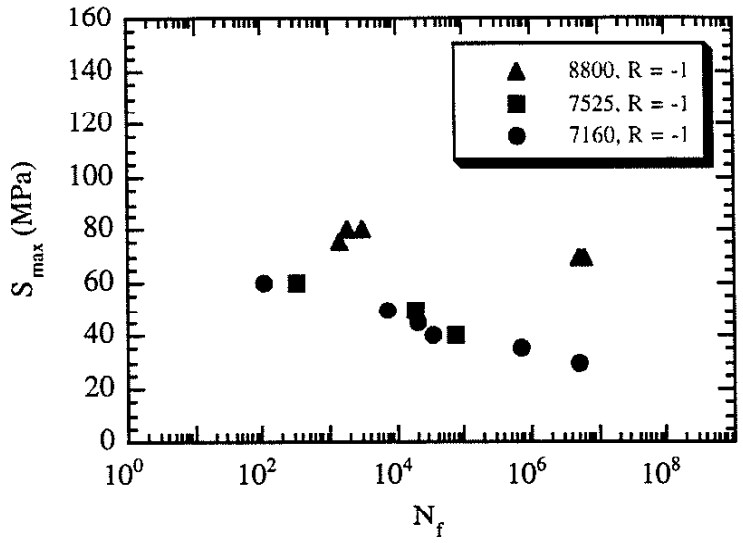

Figure 4.8 The maximum loading stress vs. fatigue life, R = -1 loading for 7160, LP7525, Quantum 8800.

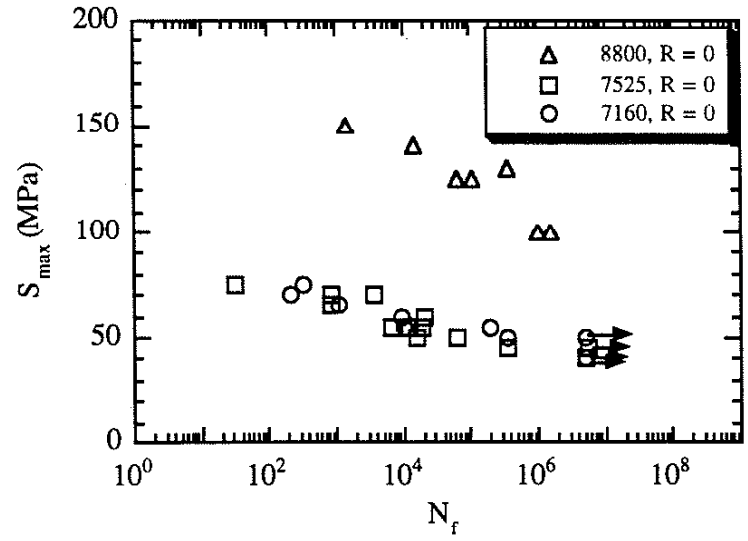

Figure 4.9 The maximum loading stress vs. fatigue life, R ≈ 0 loading for 7160, LP7525, Quantum 8800.

Figure 4.6 and 4.7 are plots of the SMC composites (FS3001, HF3502, and FS4501) which were manufactured by Navistar Corporation with R=-1 and R≈0 loading, respectively. In both figures, FS4501 (45% glass fiber) had the highest fatigue life of the three composites; FS3001 (30% glass fiber) had the lowest fatigue life. Figure 4.8 and 4.9 are plots of the SMC composites (7160, LP7525, and Quantum 8800) which were manufactured by GenCorp with R=-1 and R≈0 loading, respectively. In both R=-1 and R≈0 loading, Quantum 8800 (62% glass fiber) had a much higher fatigue life than the other SMC composites. It is interesting to note that Quantum 8800 shows considerable improvement in life. The 7160 and LP7525 composites had very similar fatigue lives; both materials contained 27% glass fiber.

4.3 Observations of Fatigue Damage

SEM (Scanning Electron Microscope) was used to obtain the microstructural damage information on SMC. The SEM photograph of the specimen is a representation of a bigger picture. Thus, it is important to sample a large volume including many fibers. Figure 4.10 and 4.11 are two of the digitized SEM photographs taken from FS4501 interrupted experiments (other SEM photographs are shown in Appendix B3). The purpose of performing image analysis on interrupted experiments was to capture the microstructural damages at different stages of the specimen life. In both experiments the stress was cycled from a maximum value of +60 MPa to a minimum value of -60 MPa. In Figure 4.10, the fatigue experiment was conducted up to 3,000 cycles, and the specimen was sectioned for viewing in the SEM. In Figure 4.11, the fatigue experiment was stopped at 7,180 cycles, and again the specimen was sectioned for viewing in the SEM.

The light gray areas with long strand shapes are the glass fibers. The light gray areas with polygon shapes are the calcium carbonate fillers, and the dark gray background

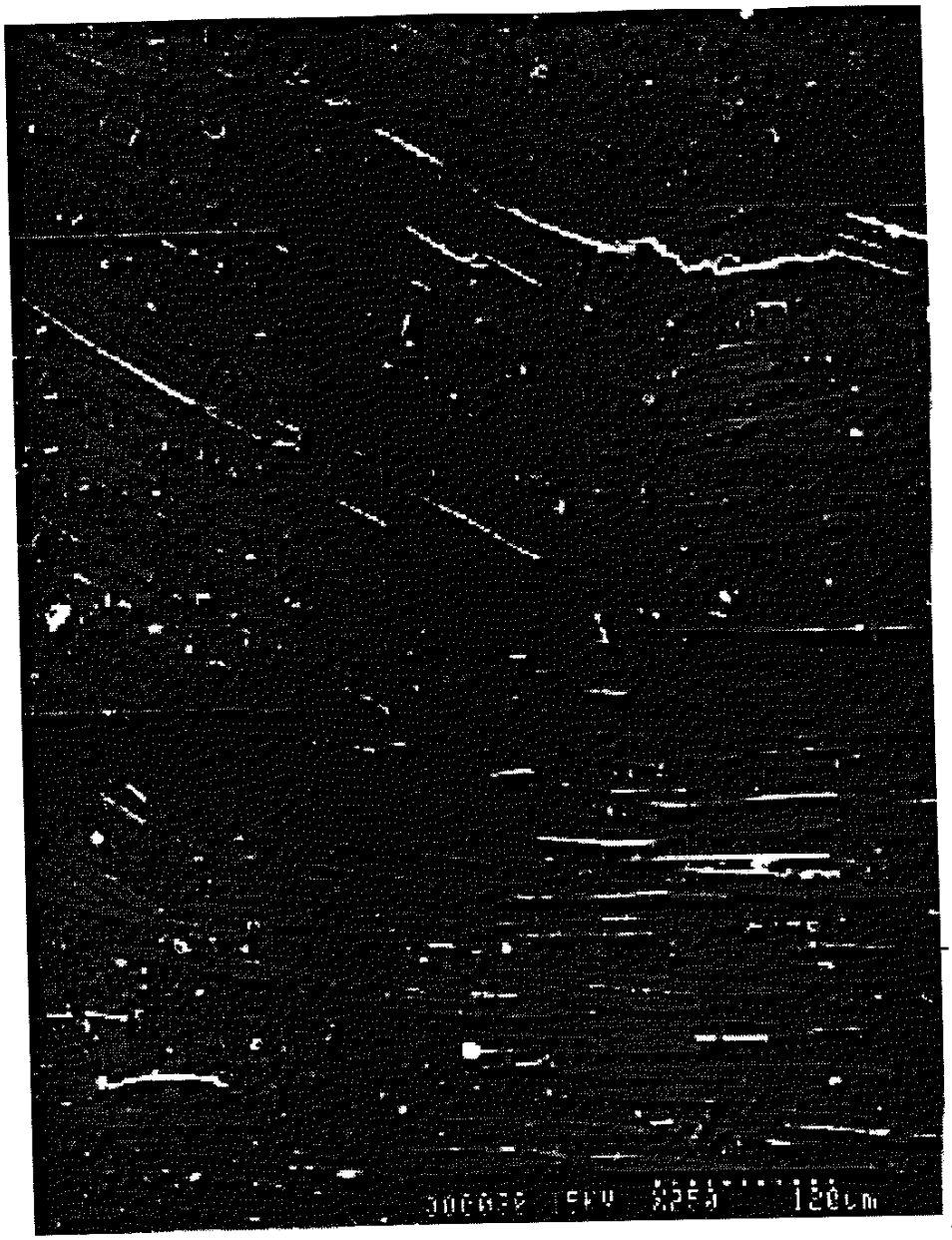

Figure 4.10 Digitized SEM photograph of FS4501 interrupted experiment (N=3000 cycles)

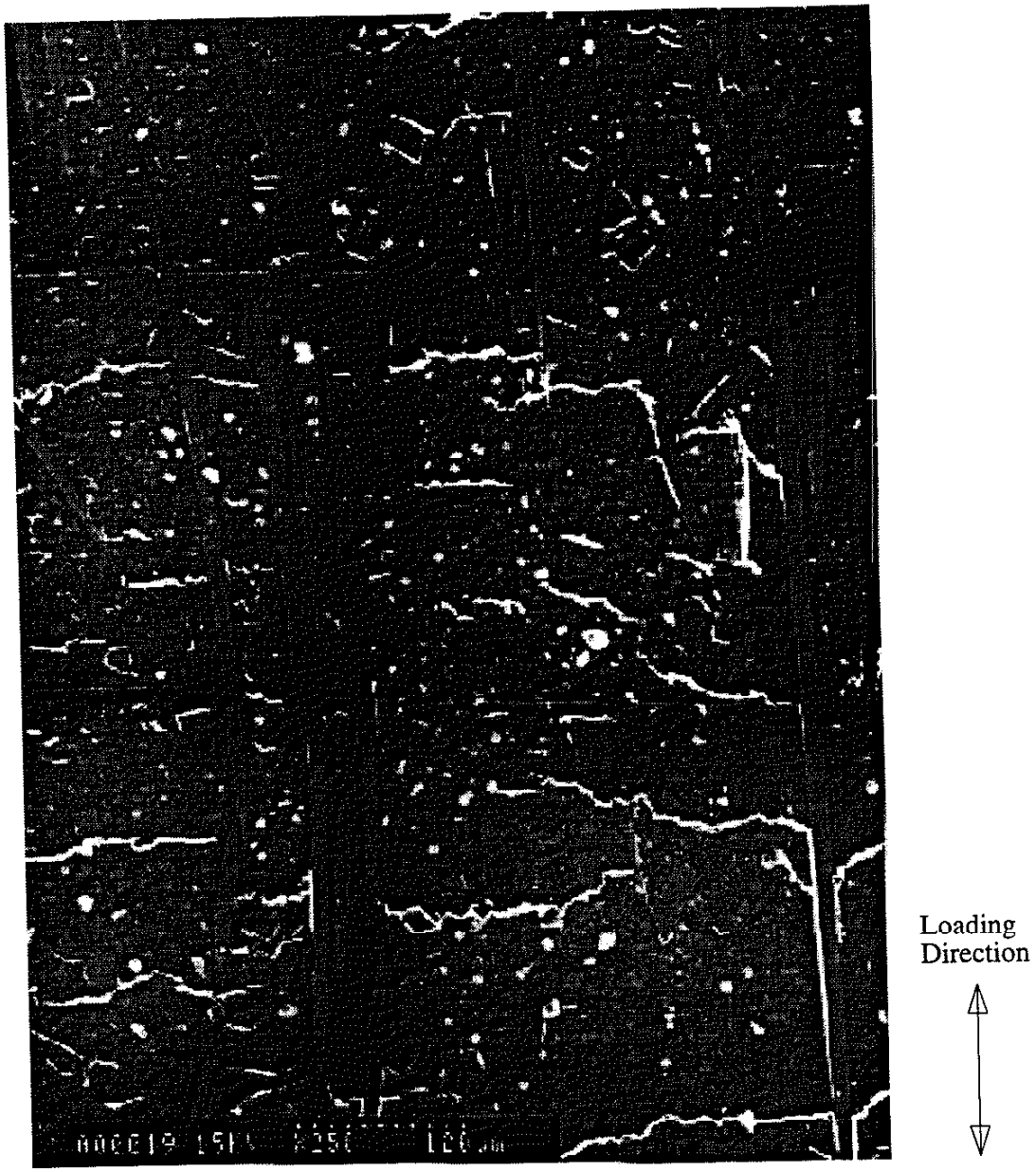

Figure 4.11 Digitized SEM photograph of FS4501 interrupted experiment (N=7180 cycles)

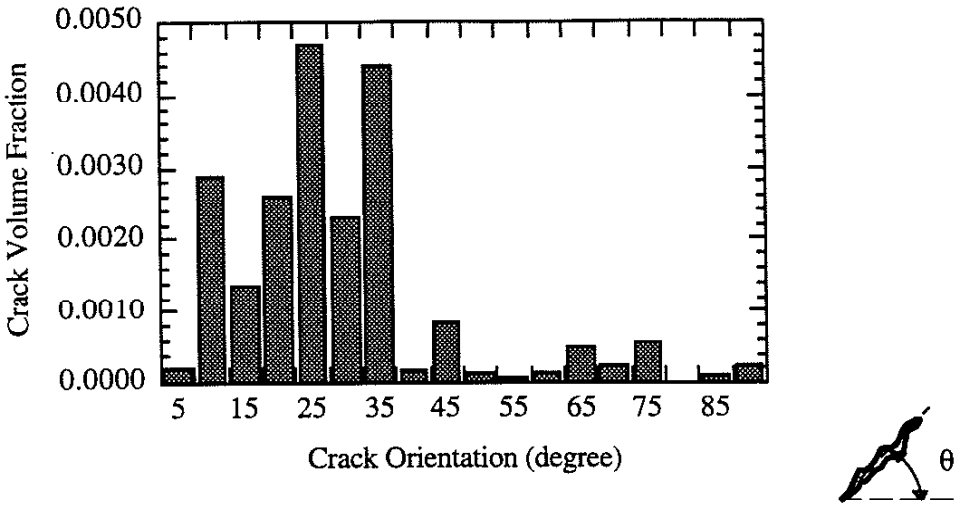

Figure 4.12 Crack distribution for FS4501 interrupted experiment, (N=3000 cycles, total volume fraction = 2.02%).

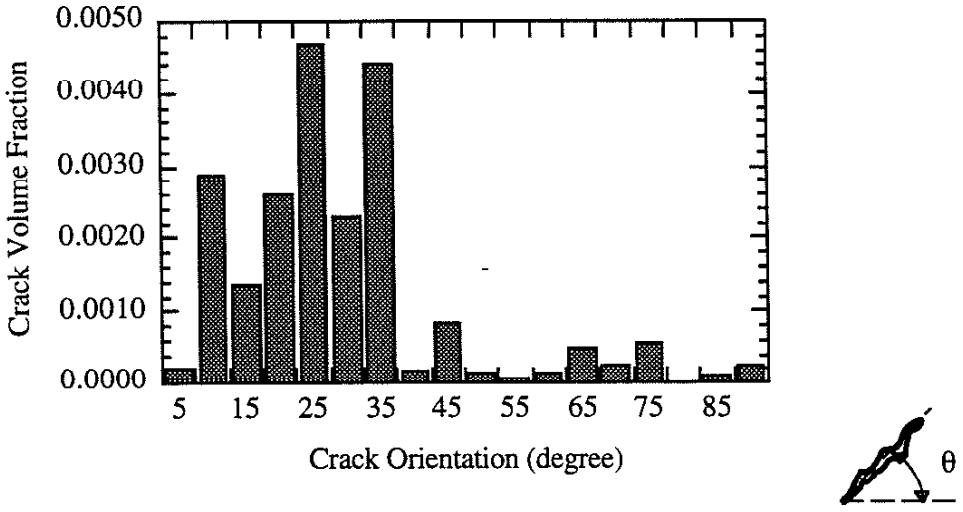

Figure 4.13 Crack distribution for FS4501 interrupted experiment, (N=7180 cycles, total volume fraction = 5.50%).

is the resin matrix. Finally, the white areas are the fatigue cracks. Comparing the volume fractions (area fractions) of the fatigue cracks in Figure 4.10 and 4.11, we note that the N=7,180 cycles experiment had significantly higher percentage of cracks than the N=3,000 cycles experiment.

The fatigue cracks initiated at the fiber-matrix interfaces or at the filler-matrix interfaces, and the crack growth continued across the matrix with increased number of cycles. This can be seen from both Figure 4.10 and 4.11. Figure 4.12 and 4.13 are plots of crack volume fraction vs. crack orientation of the same experiments (N=3,000 cycles and N=7,180 cycles, respectively). The crack orientation was measured with respect to the horizontal axis,. For instance, a crack orientation of 0° represents the crack being perpendicularly aligned with the loading axis. The loading patterns in both experiments were aligned with the vertical direction of the figures. Figure 4.12 and 4.13 shows that the cracks are not randomly distributed and are directionally dependent on the loading direction. Most of the crack orientations are within 35° of the normal to the loading direction. The total crack volume fraction in Figure 4.12 (N=3000 cycles) is 2.02% compared to 5.50% in Figure 4.13 (N=7180 cycles).

The information gathered in Figure 4.12 and 4.13 is later used in modulus simulations. Each crack orientation along with the corresponding volume fraction are being considered as different types of inclusions in the composite. The overall modulus is heavily dependent on both the volume fraction and orientation of all the cracks. The details of the modulus simulation are explained in section 5.1.

5. Modeling Results and Comparison with Experiments

5.1 Determination of Modulus Degradation in the presence of Fatigue Damage

The fatigue life of SMC directly depended on the microstructural damages of the composite. As the microstructural damages increased with the number of cycles, the modulus decreased during the fatigue life. It is important to be able to predict the specimen modulus by investigating the fatigue damage information. Consequently, the modulus prediction can be used to estimate the remaining fatigue life of the specimen.

In this study, the Modulus Prediction Program was written based on the Eshelby's equivalent inclusion method and the Mori-Tanaka's analysis. A copy of the Modulus Prediction Program is available in Appendix C. The overall modulus of a composite with ellipsoidal inhomogeneities (in this study, cracks) can be solved once the corresponding eigenstrains are solved by using the Eshelby's equivalent inclusion method. However, when the volume fraction of inhomogeneities becomes large the Eshelby's equivalent inclusion method does not account for the interaction effects. Therefore, the Mori-Tanaka's method is incorporated into the program to take into account the interaction among the inhomogeneities when the volume fraction of inhomogeneities becomes large.

There are two major assumptions in the Modulus Prediction Program. The first assumption is that the program is written for a composite with ellipsoidal cracks having the width much smaller than the length. However, the program can be easily modified for the other shapes of crack by changing the formulas for the Eshelby tensor. The second assumption is that the composite is a planar isotropic material; SMC is a planar isotropic composite with randomly distributed fibers in the planar surface.

To apply the program, first of all, the inputs needed are the volume fraction, orientation angle, width, and length of each crack orientation. The information is obtained

from the digitized SEM (Scanning Electron Microscope) photographs of tested specimen using the NIH Image Analysis software. Note that the Modulus Prediction Program is not limited to any number of cracks. The size of the arrays can be easily set up by changing the parameter number in the program. Once the fatigue damage information is stored, the program calculates the Eshelby and stiffness tensors needed for computations. The next step is solving for the eigenstrains of each crack orientation. The details of the formulations can be seen in section 3.2. After the computations of eigenstrains, the last step is using the equivalence of the strain energies to calculate the overall modulus of the fatigue damaged specimen. The calculated overall modulus is actually the longitudinal modulus of the composite; it is the modulus value in the loading direction.

5.2 Modulus Simulation Results

Several interrupted FS4501 cyclic experiments were conducted to determine the microstructural damages at various stages of the specimen life. The purpose of performing these tests is to develop a onetime correlation between modulus, life, and the image obtained from the specimen. The results of simulations and experimental values are shown in Figure 5.1 by plotting normalized modulus (final modulus / initial modulus) vs. crack volume fraction. The modulus predictions were very close to the actual experimental values; the differences were less than 9% of the experimental values. The above results were plotted again in Figure 5.2 showing normalized modulus vs. number of cycles. There were only three experimental values on this figure. The curve in Figure 5.2 was not a smooth curve due to the fact that the N=7,180 cycles experiment failed earlier than expected. Theoretically, a N=7,180 cycles experiment should have a lower crack volume fraction and thus resulting in a higher modulus prediction. In order to use the figures above for later references, more experiments need to be conducted to get a complete representation of the correlation between the modulus degradation and the fatigue life.

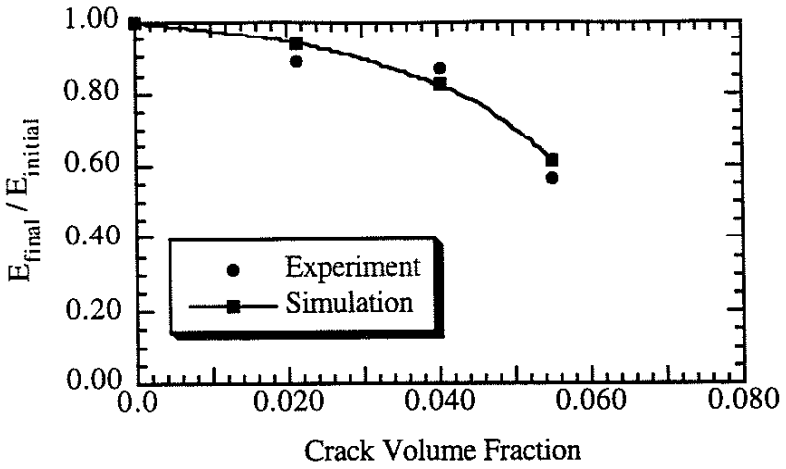

Figure 5.1 Modulus simulation results, normalized modulus vs. crack volume fraction. (FS4501, R=-1, ΔS=120 MPa loading)

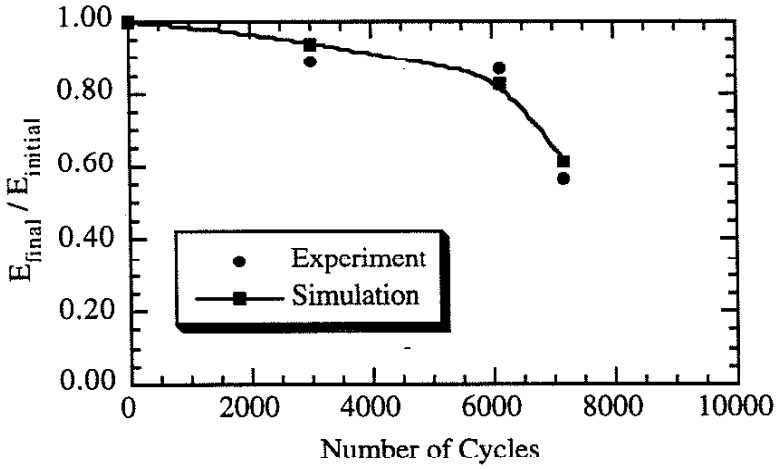

Figure 5.2 Modulus simulation results, normalized modulus vs. number of cycles. (FS4501, $N_f \approx 60{,}000$ cycles, R=-1, ΔS=120 MPa loading)

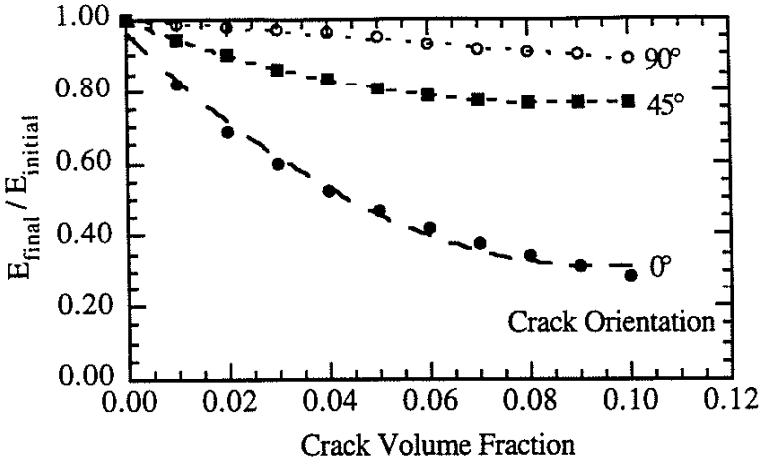

Figure 5.3 Modulus simulation results for crack orientations of 0°, 45°, and 90°.

The modulus prediction was greatly affected by the crack volume fraction. In addition, the crack orientation angle was also a major factor in modulus simulation. The results of three simulated specimens each with only one type of crack orientation angle were compared in Figure 5.3. As expected, the specimen with crack orientation angle of 0° (perpendicular to the loading direction) had the most degradation in modulus; the specimen with crack orientation angle of 90° (aligned with the loading direction) had the least degradation in modulus. In this study, most of the fatigue cracks were perpendicularly aligned to the loading directions or followed the fiber matrix interfaces. Therefore, the modulus degradation is not only affected by the crack volume fraction, it heavily depended on the crack orientation distribution.

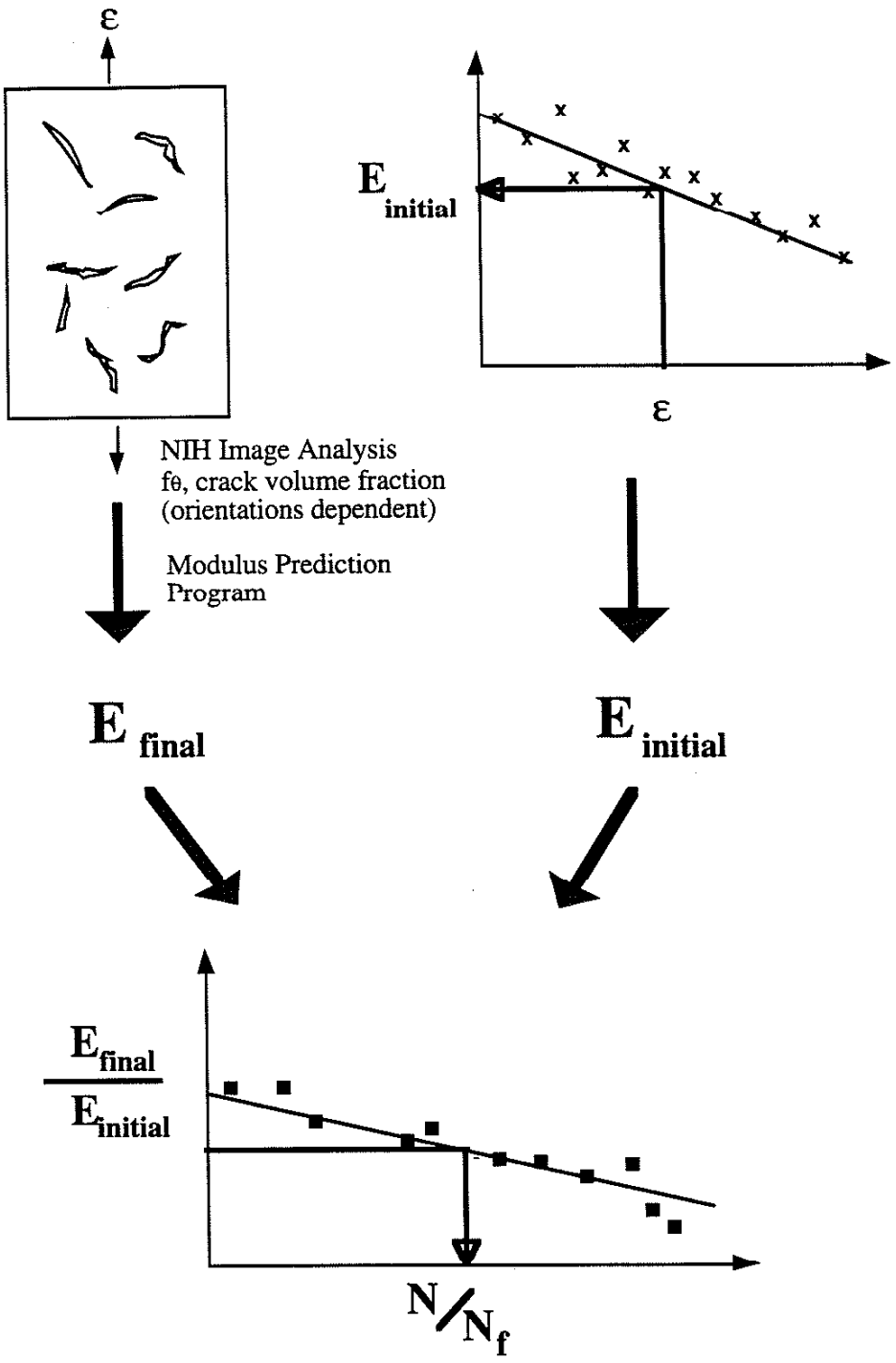

Figure 5.4 Schematic of remaining life estimation procedure

5.3 Remaining Life Estimation of SMC composites

In addition to using the Modulus Prediction Program, the procedure for estimating remaining life of SMC composites involves additional correlations between the modulus, applied strain, and life. A schematic of the proposed procedure for life estimation is shown in Figure 5.4. A replica containing the damage information is attained from a specimen or serviced part. Once the damage information is obtained from the replica, the modulus degradation modeling can be performed to predict the final modulus value. The previous experiments have shown that the initial modulus of SMC varied greatly depending on the selected applied strain. A correlation of initial modulus vs. applied strain (obtained experimentally) is needed to obtain the initial modulus value. The applied strain, ε, on the part is available from a strain gage reading or other strain measurement technique. From knowing both the initial modulus and final modulus values, the remaining life of the SMC specimen or serviced part can be determined by using the normalized modulus vs. life plot.

6. Conclusions

(1) The SMC composites' mechanical properties vary greatly depending on the volume fractions of glass fiber. Quantum 8800 with 62% glass fiber has the highest fracture strength and initial modulus of 270 MPa and 17,601 MPa, respectively; LP7525 with 27% glass fiber has the lowest fracture strength and initial modulus of 84 MPa and 8,578 MPa, respectively. All six SMC composites are very brittle with low fracture strains of approximately 1% to 2%.

(2) The modulus of SMC decreases with increasing number of cycles. In addition, the modulus degradations occur not only as a function of fatigue cycles, but also at different locations of the hysteresis loop within one cycle.

(3) FS4501 has the highest fatigue life and FS3001 has the lowest fatigue life among the Navistar materials. Quantum 8800 has a much higher fatigue life than 7160 and LP7525 of the GenCorp materials. Both 7160 and LP7525 have very similar fatigue life.

(4) The failure mechanisms in SMC are the fiber-matrix debonding, filler-matrix debonding, and matrix cracking. The fatigue damage initiates at the fiber-matrix interfaces and the filler-matrix interfaces. The fatigue cracks are not randomly oriented and are generally aligned within 35° of the normal to the loading direction.

(5) The Modulus Prediction Program is written based on Eshelby's equivalent inclusion method and Mori-Tanaka's analysis. The modulus predictions of the program are very accurate compared to the experimental values. The largest

difference between the predictions and the experimental results is 9%. However, to complete the correlation of modulus and life, more experimental data is needed. A procedure is outlined for estimating the remaining life of the SMC composite using photograph obtained on the surface and the Modulus Prediction Program.

References

1. Advani, S. G., "Prediction of fiber orientation during processing of short fiber composites", Ph.D. Thesis, Department of Mechanical and Industrial Engineering, University of Illinois, Champaign-Urbana, Illinois, (1987).

2. Chim, E. S., "Tensile fatigue damage and degradation of random short-fiber SMC composite", Ph.D. Thesis, Department of Mechanical and Industrial Engineering, University of Illinois, Champaign-Urbana, Illinois, (1985).

3. Mura, Toshio, "Micromechanics of defects in solids" Martinus Nijhoff Publishers, (1982).

4. Eshelby, J. D., "The determination of the elastic field of an ellipsoidal inclusion, and related problems", *Proc. R. Soc. (London)*, Vol. A241, pp. 376-396, (1957).

5. Mori, T. and Tanaka, K., "Average stress in matrix and average elastic energy of materials with misfitting inclusions", *Acta Metallurgica* 21, pp. 571-574, (May 1973).

6. Taya, M. and Chou, T., "On two kinds of ellipsoidal inhomogeneities in an infinite elastic body: an application to a hybrid composite", *Int. J. Solids Structures*, Vol. 17, pp. 553-563, (1981).

Appendix A: Experiment Summary

Table A.1 Tensile Experiment Summary

Material	Specimen ID	E (MPa)	σ_f (MPa)	ε_f
FS3001	-8	11,656	110	0.013
HF3502	-8	14,563	130	0.014
FS4501	1-1	16,830	137	0.024
7160	5-1	11,178	98	0.024
7160	6-2	11,257	89	0.015
LP7525	5-2	9,167	78	0.0165
LP7525	6-3	7,990	89	0.025
Quantum 8800	7-1	16,512	276	0.0235
Quantum 8800	8-3	18,681	265	0.0198

Table A.2 Fatigue Experiment Summary for FS3001

Specimen ID	Frequency (Hz)	σ_{max} (MPa)	σ_{min} (MPa)	Nf (cycles)
-6	5	50	5	2062971
-7	5	40	-40	6525901
-11	3	70	5	47306
-12	2.5	60	5	221232
-13	2.5	60	0	11489
-14	5	45	-45	4931275
-15	2.5	70	-70	169
-16	5	50	5	>1200000
-17	5	40	-40	>1337247
-18	5	50	-50	183023
-19	3	50	-50	7319
-20	3	40	5	>1100000

Table A.3 Fatigue Experiment Summary for HF3502

Specimen ID	Frequency (Hz)	σ_{max} (MPa)	σ_{min} (MPa)	Nf (cycles)
-5	5	50	5	468675
-6	5	60	5	2933273
-11	2.5	80	5	2051
-12	2.5	90	5	85
-13	5	45	-45	469937
-14	5	50	-50	237157
-15	5	40	-40	2763533
-16	5	60	-60	52578
-17	5	70	-70	18889
-18	5	70	5	88492
-19	5	50	-50	>1675967
-20	5	60	5	>1100000
1-1	5	60	5	2014556
1-2	5	50	5	>5581658

Table A.4 Fatigue Experiment Summary for FS4501

Specimen ID	Frequency (Hz)	σ_{max} (MPa)	σ_{min} (MPa)	N_f (cycles)
-3	5	55	-55	692
-4	5	55	-55	8778
-7	5	70	5	194
-11	2.5	80	-80	2416
-12	2.5	90	5	4365
-13	2.5	80	5	55901
-14	2.5	100	5	3042
-15	2.5	90	-90	884
-16	3	50	-50	>1717946
-17	5	60	5	>1030628
-18	5	70	5	>1055106
-19	3	70	-70	13731
-20	5	60	-60	69336
1-3	5	60	-60	6914604
2-1	5	55	-55	2392415
2-3	2.5	70	5	32586
3-2	5	60	-60	51746
5-2	1	80	-80	7447

Table A.5 Fatigue Experiment Summary for 7160

Specimen ID	Frequency (Hz)	σ_{max} (MPa)	σ_{min} (MPa)	N_f (cycles)
1-1	5	45	-45	20047
1-2	2.5	60	5	9519
1-3	5	35	-35	725668
2-1	2.5	50	-50	7099
2-2	5	30	-30	>5130144
2-3	5	55	5	201459
3-1	1	60	-60	104
3-2	5	45	5	>5182257
3-3	5	45	5	>6000000
4-1	2.5	50	5	342470
4-2	2.5	65	5	1070
4-3	2.5	40	-40	33954
5-2	5	50	5	>5168738
5-3	5	55	5	9885
6-1	1	70	5	215
6-3	5	40	5	>5234094
7-1	1	75	5	330
7-2	1	60	-60	200

Table A.6 Fatigue Experiment Summary for LP7525

Specimen ID	Frequency (Hz)	σ_{max} (MPa)	σ_{min} (MPa)	Nf (cycles)
1-1	5	43.3	4.8	>5533376
1-2	2.5	70	5	3685
1-3	1	60	-60	317
2-1	2.5	60	5	20351
2-2	2.5	50	-50	18984
3-1	2.5	70	5	862
3-2	1	75	5	32
3-3	5	45	5	364340
4-1	2.5	65	5	833
4-2	2.5	50	5	62996
4-3	2.5	40	-40	73339
5-1	2.5	40	5	>5000000
5-3	2.5	55	5	12768
6-1	2.5	55	5	6970
6-2	2.5	50	5	15205
7-3	5	55	5	18453

Table A.7 Fatigue Experiment Summary for Quantum 8800

Specimen ID	Frequency (Hz)	σ_{max} (MPa)	σ_{min} (MPa)	Nf (cycles)
1-1	2.5	140	5	15047
1-2	5	70	-70	>6004145
1-3	1	130	5	357123
2-1	1	150	5	1410
2-2	2.5	75	-75	1716416
2-3	5	75	-75	1444
3-3	1	80	-80	21319
4-3	1	90	-90	4269
5-3	1	85	-85	12031
7-2	5	100	5	1489886
7-3	5	125	5	106056
8-1	5	70	-70	4955671
8-2	5	80	-80	1863
9-1	5	80	-80	3021
9-2	5	100	5	1013065
9-3	2.5	125	5	62420

Appendix B: Experimental Figures

B.1 Tensile Experiments

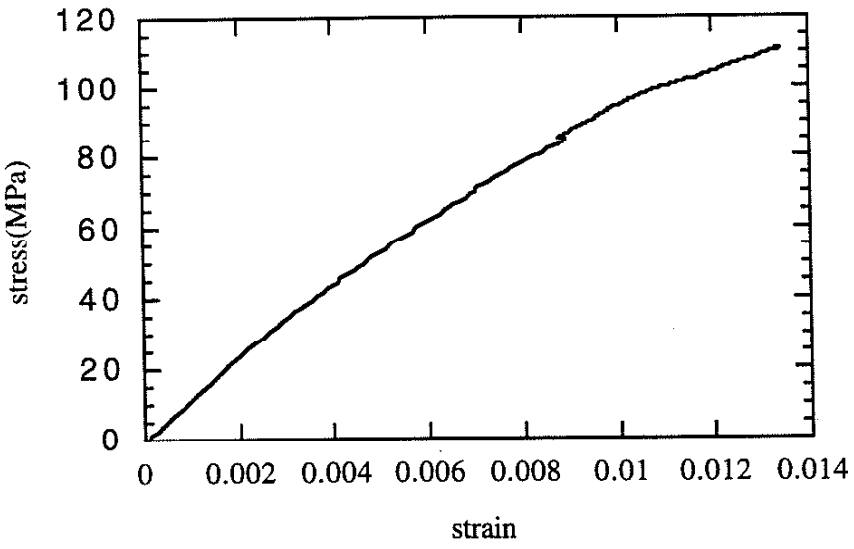

Figure B.1 Tensile experiment result of FS3001, stress vs. strain.

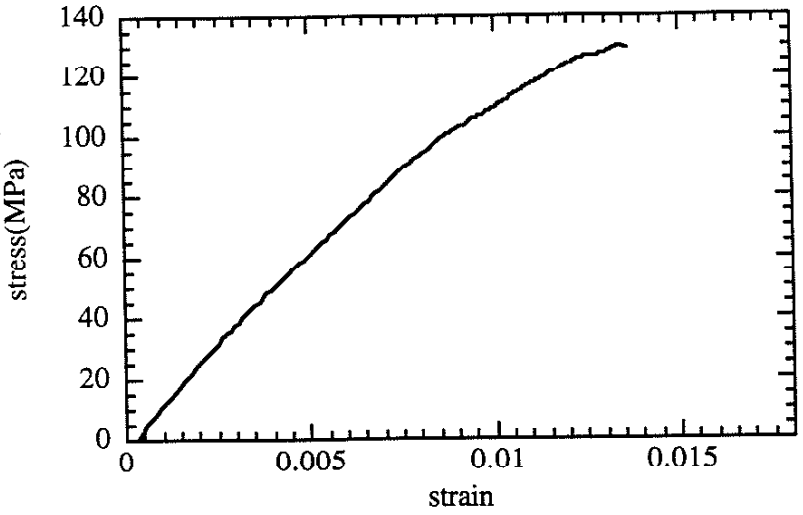

Figure B.2 Tensile experiment result of HF3502, stress vs. strain.

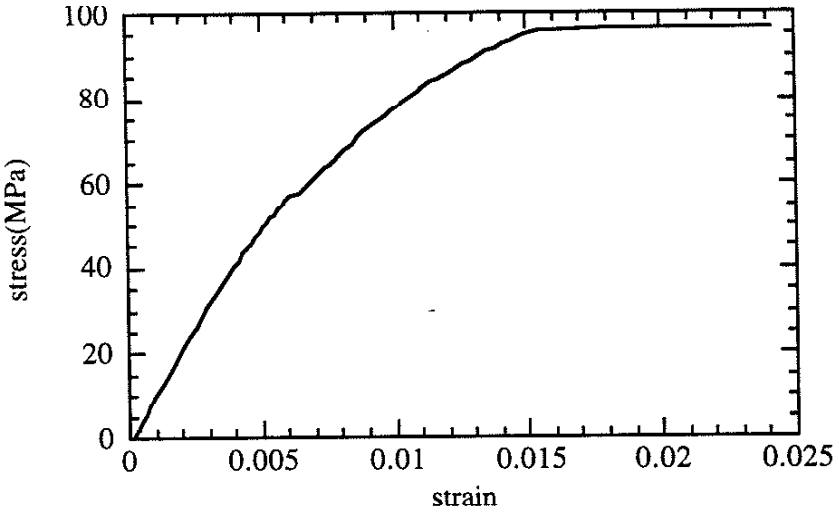

Figure B.3 Tensile experiment result of FS4501, stress vs. strain.

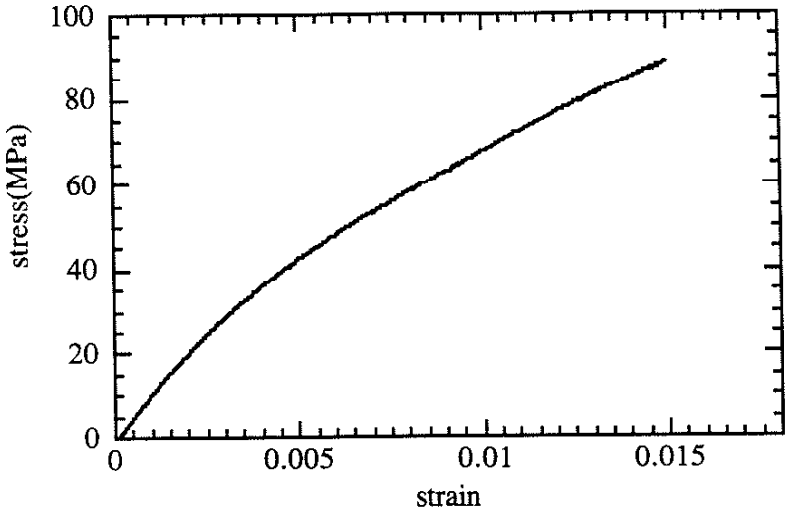

Figure B.4 Tensile experiment result of 7160, stress vs. strain.

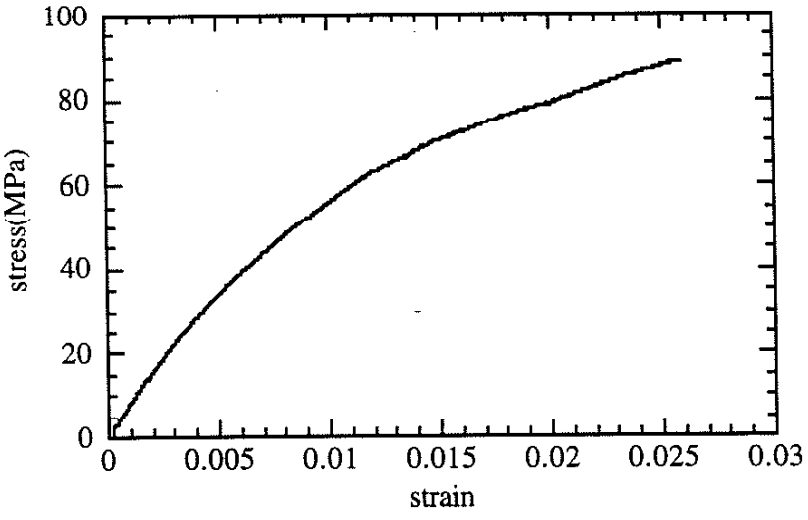

Figure B.5 Tensile experiment result of LP7525, stress vs. strain.

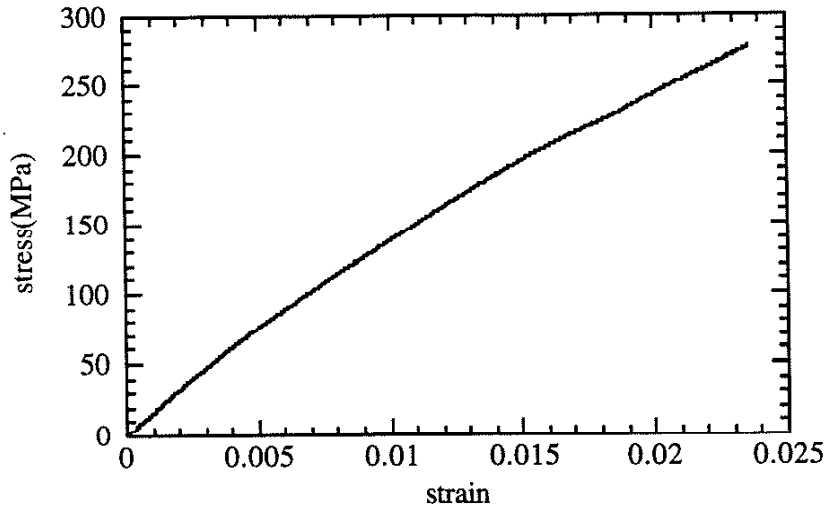

Figure B.6 Tensile experiment result of Quantum 8800, stress vs. strain.

B.2 Fatigue Experiments

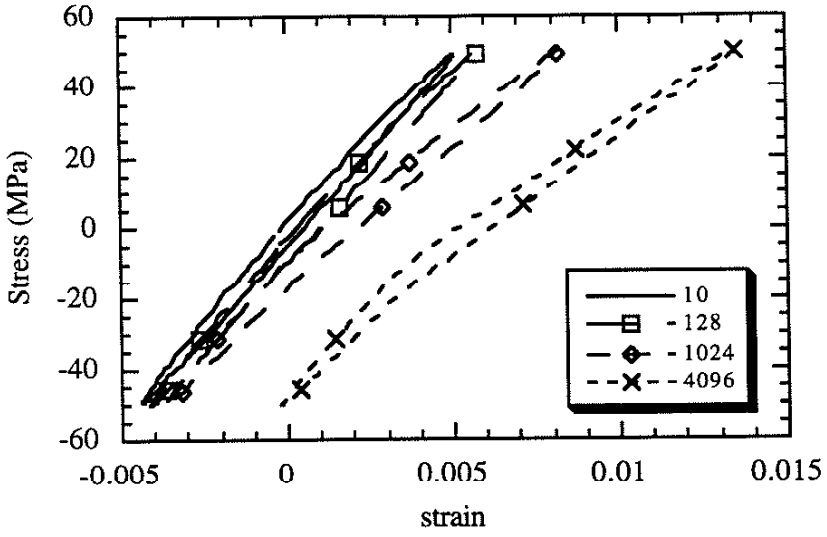

Figure B.7 Stress-strain behavior of FS3001 under R=-1, ΔS=100 MPa loading (Frequency=3Hz, N_f=7,319).

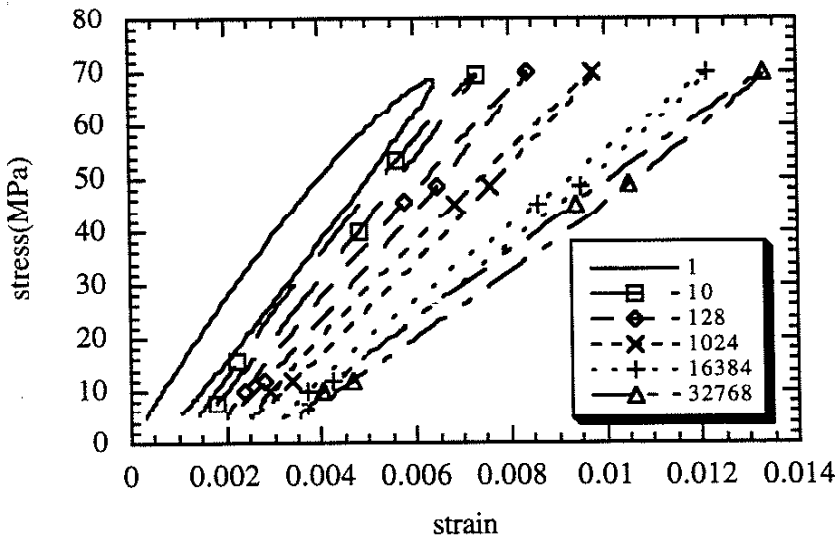

Figure B.8 Stress-strain behavior of FS3001 under R=0, ΔS=65 MPa loading (Frequency=3Hz, N_f=47,306)

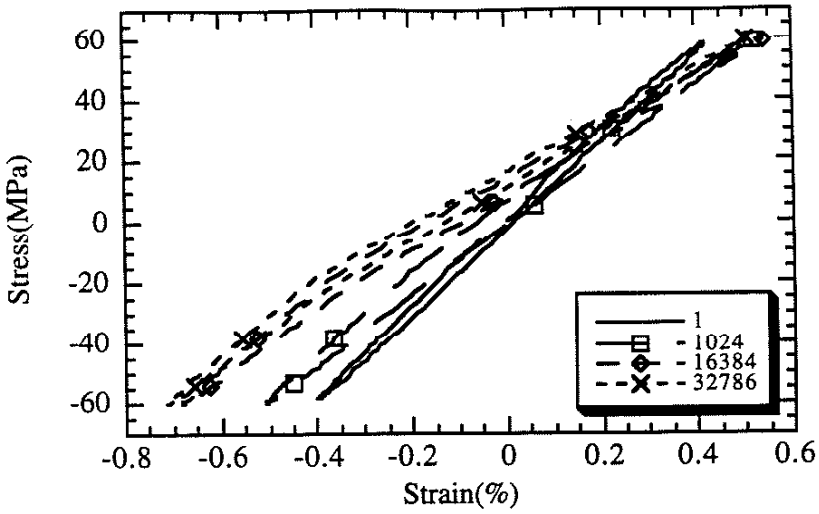

Figure B.9 Stress-strain behavior of HF3502 under R=-1, ΔS=120 MPa loading (Frequency=5Hz, N_f=52,578).

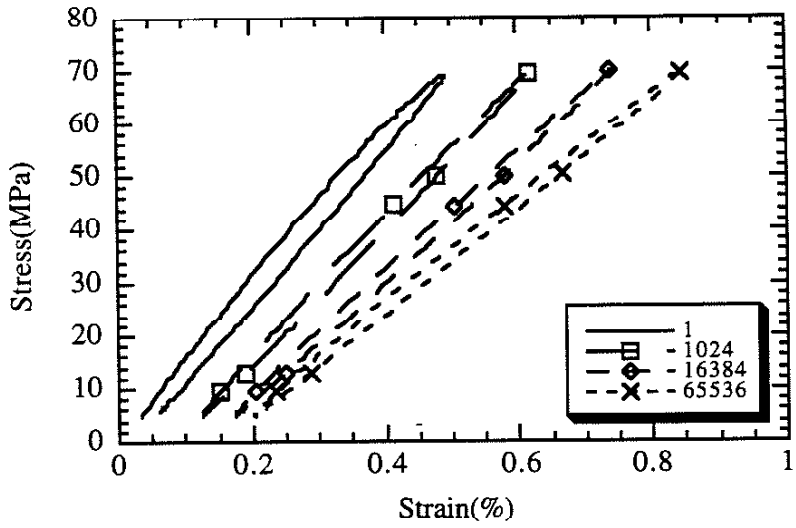

Figure B.10 Stress-strain behavior of HF3502 under R≈0, ΔS=65 MPa loading (Frequency=5Hz, N_f=88,492)

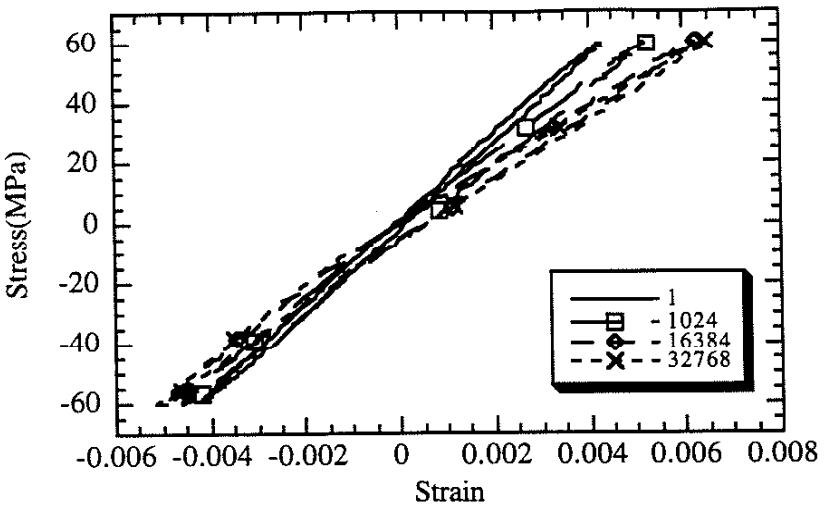

Figure B.11 Stress-strain behavior of FS4501 under R=-1, ΔS=120 MPa loading (Frequency=5Hz, N_f=51,746).

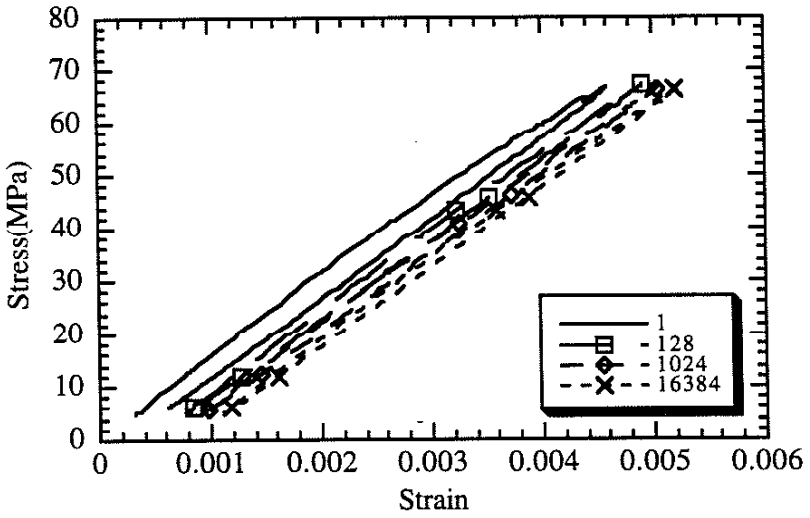

Figure B.12 Stress-strain behavior of FS4501 under R≈0, ΔS=65 MPa loading (Frequency=2.5Hz, N_f=32,586)

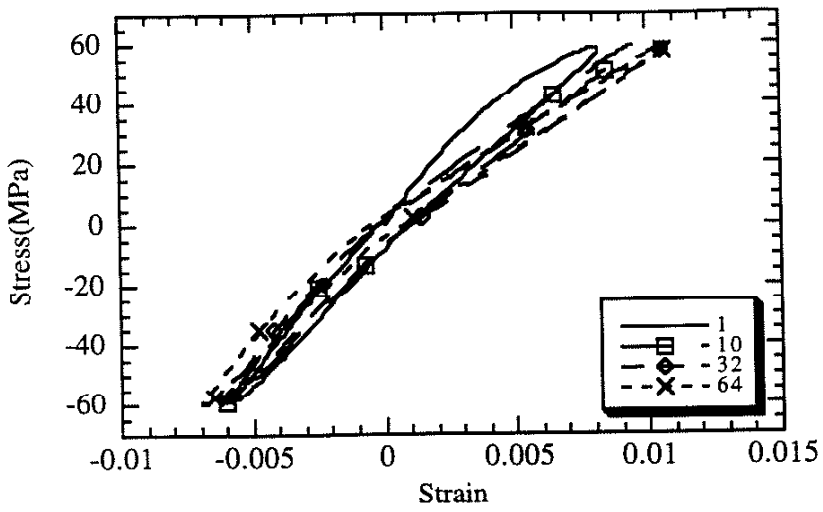

Figure B.13 Stress-strain behavior of 7160 under R=-1, ΔS=120 MPa loading (Frequency=1Hz, N_f=104).

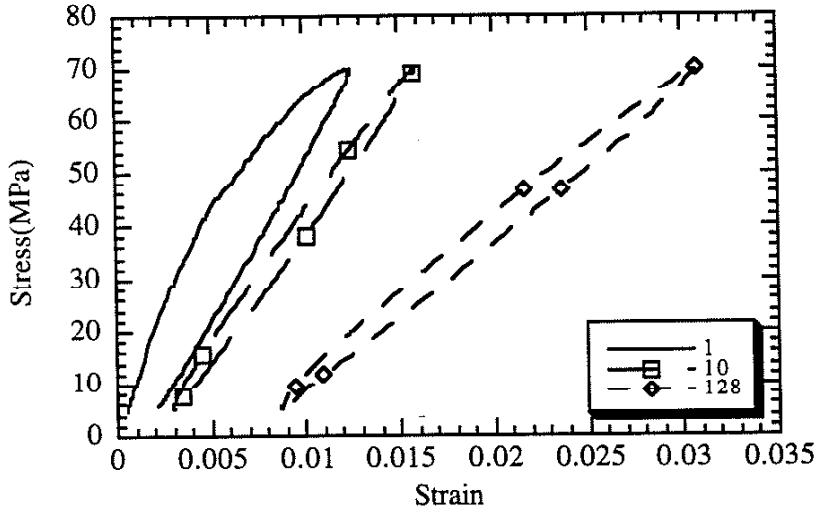

Figure B.14 Stress-strain behavior of 7160 under R≈0, ΔS=65 MPa loading (Frequency=1Hz, N_f=215)

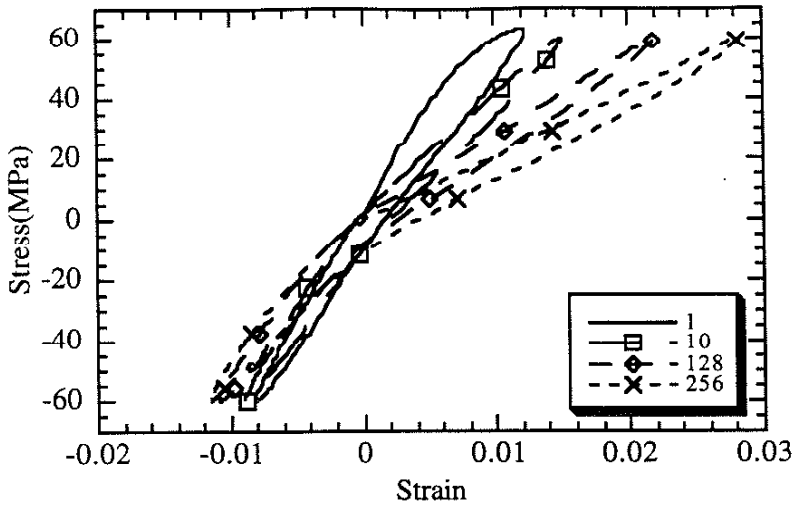

Figure B.15 Stress-strain behavior of LP7525 under R=-1, ΔS=120 MPa loading (Frequency=1Hz, N_f=317).

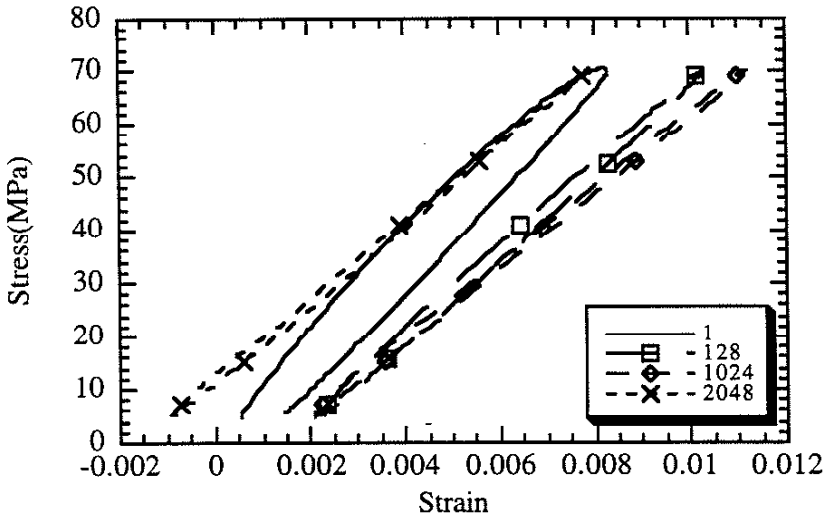

Figure B.16 Stress-strain behavior of LP7525 under R≈0, ΔS=65 MPa loading (Frequency=2.5Hz, N_f=3,685)

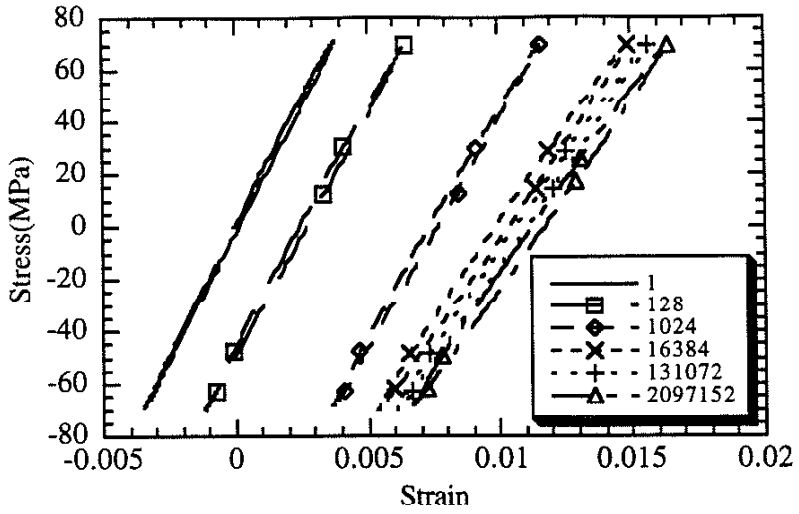

Figure B.17 Stress-strain behavior of Quantum 8800 under R=-1, ΔS=140 MPa loading (Frequency=5Hz, N_f=4,955,671).

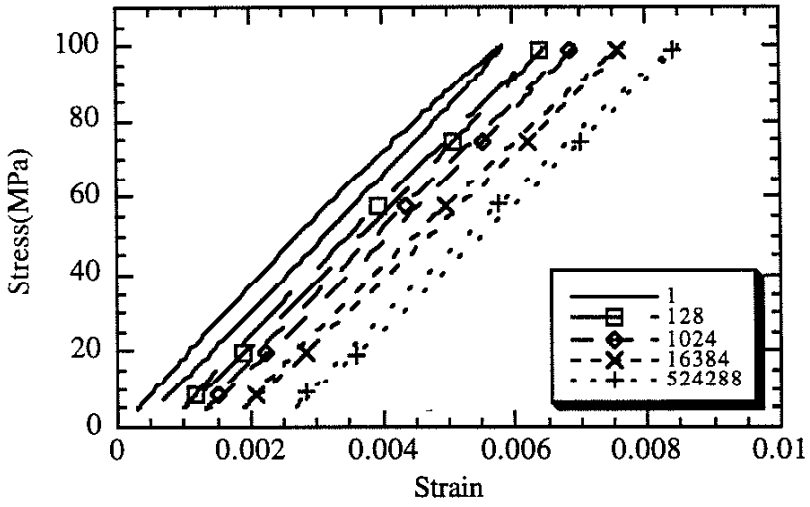

Figure B.18 Stress-strain behavior of Quantum 8800 under R≈0, ΔS=95 MPa loading (Frequency=5Hz, N_f=62,420)

B.3 Scanning Electron Microscope Photographs

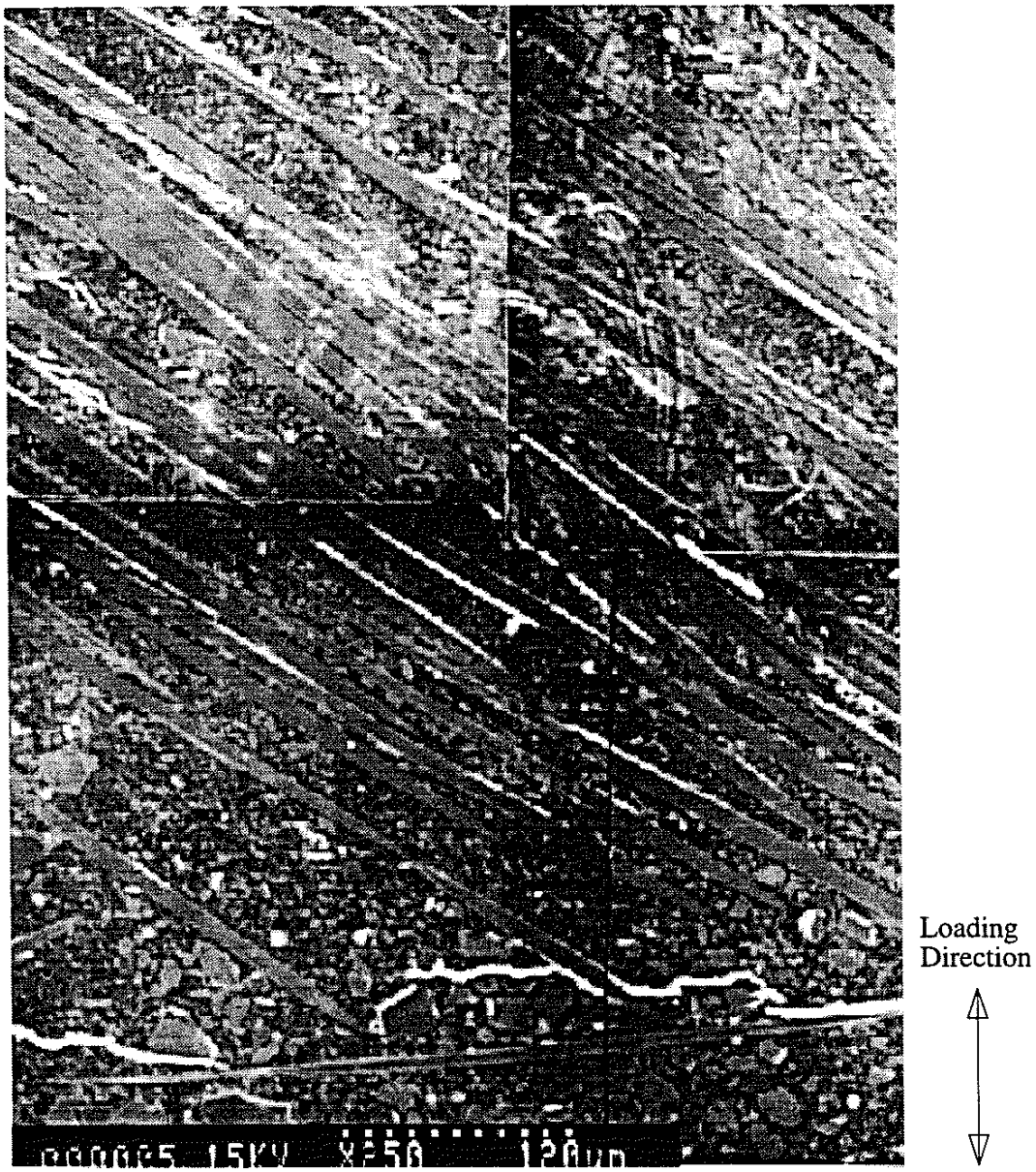

Figure B.19 Digitized SEM photograph of FS4501 interrupted experiment (N=6000 cycles)

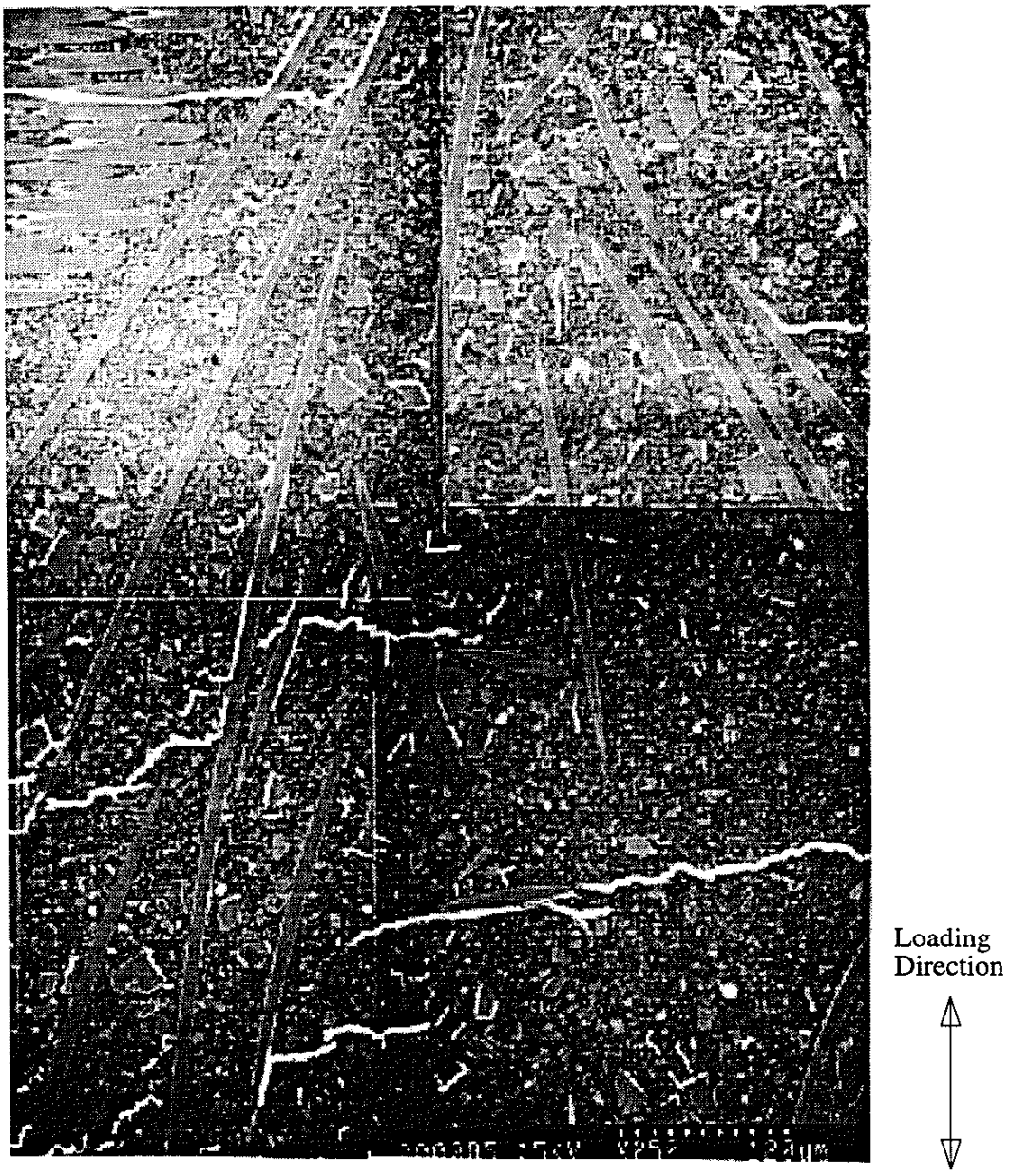

Figure B.20 Digitized SEM photograph of FS4501 interrupted experiment (N=15,000 cycles)

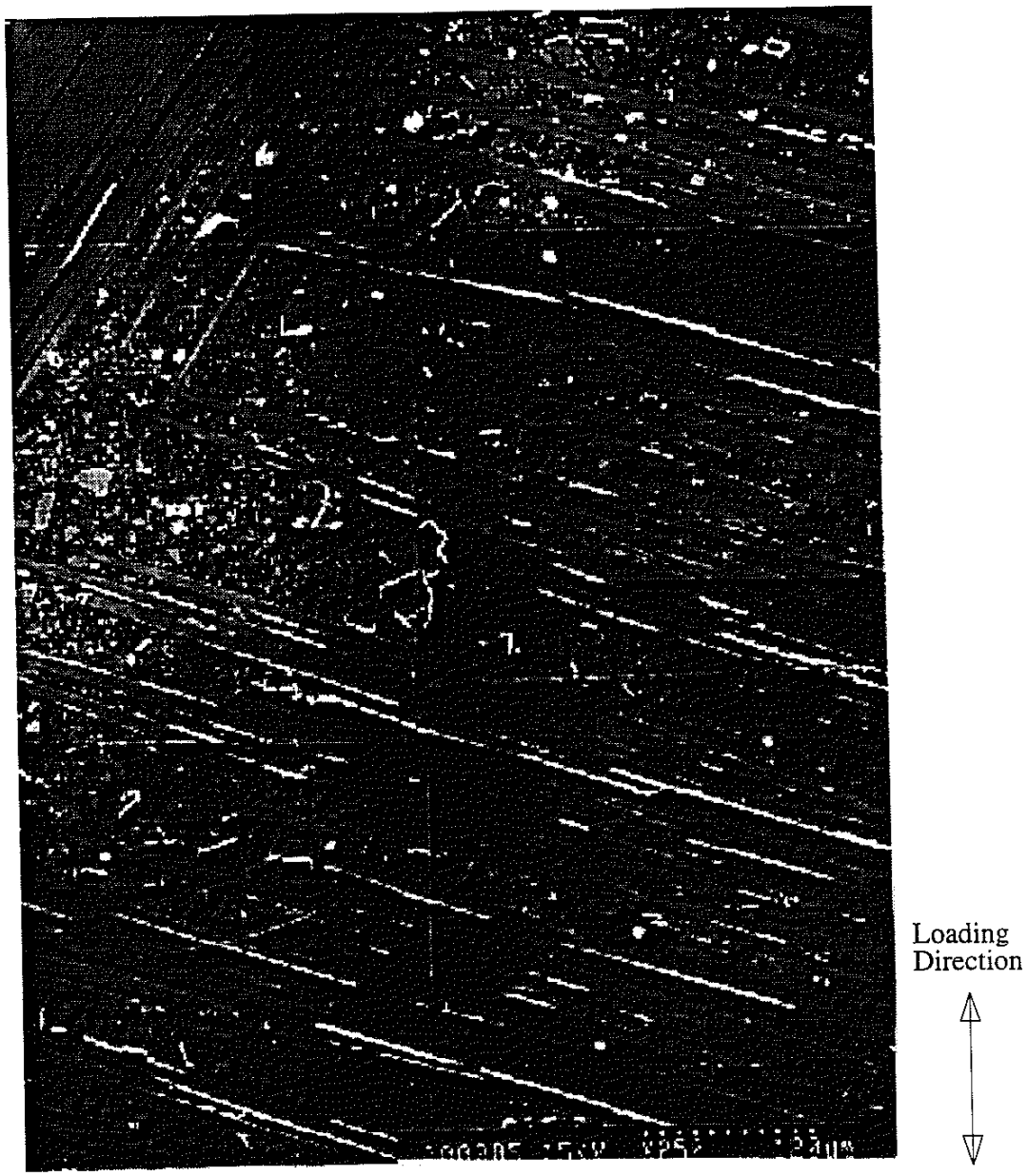

Figure B.21 Digitized SEM photograph of FS4501 interrupted experiment (N=51,746 cycles)

Appendix C: Modulus Prediction Program Code

```
      Program Modulus

      integer num
      parameter (max=1000)
      real mod,v32,v31,v12,G23
      real x,y,z
      real vf(max),theta(max),a3(max),a2(max)
      real stiff(max,6,6),eshlby(max,6,6)
      real temp1(2,max),temp2(2,max),temp3(2,max)
      real tempa(max),tempb(max),tempc(max),tempd(max)
      real tempe(max),tempf(max),tempg(max),temph(max)
      real tempr(max),temps(max),tempt(max),tempu(max),tempv(max)
      real tempx1(max),tempx2(max),tempx3(max)
      real tempy1(max),tempy2(max),tempy3(max)
      real tempz1(max),tempz2(max),tempz3(max)
      real tempx(max),tempy(max),tempz(max)
      real const1(2),const2(2),const3(2)
      real estar3(max),eave22,eave33
      real modcom, modtem
      open (25, file = 'stiff.3000')
      open (26, file = 'eshelby.3000')
      open (27, file = 'result.3000')
c*************************************************************************
c     Read In Crack Volume Fractions, Orientation Angles, Aspect ratio
c*************************************************************************
      open (10, file='crackfile.3000')
      num = 1

5     read (10,*,end=9) dvf,dtheta,da3,da2
      num = num + 1
      vf(num) = dvf
      vf(1) = 1.0 - vf(num)
      theta(num) = dtheta / 180.0 * 3.14159
      a3(num) = da3
      a2(num) = da2
      goto 5
9     continue
c     write(25,*)num,dvf,dtheta,da3,da2
c*************************************************************************
c     Material Properties
c*************************************************************************
      mod = 16460.0
      v32 = 0.32
      v31 = 0.29
      v12 = v31
      G23 = 3000.0
c*************************************************************************
c     Stiffness Tensors
c*************************************************************************
```

```
      do 10 i1 = 1, 6
       do 15 i2 = 1, 6
        stiff(1,i1,i2) = 0.0
15     continue
10    continue
      x = v32
      y = v31
      z = -2 * x**2 - 2 * x**2 * y - y**2 +1
      stiff(1,2,1) = mod * (x**2 + y) / z
      stiff(1,2,2) = mod * (-3 * x**4 - 2 * x**4 *y - 3 * x**2 * y**2
     +          -5 * x**2 * y - y**2 + 2 * y + 1) / z
      stiff(1,2,3) = mod * (-2 * x**4 - 2 * x**4 * y - 3 * x**3
     +              - 3 * x**2 * y**2 - y**3 - 2 * x**2 * y
     +              - x * y**2 + x**2 + x * y + 2 * x + y) / z
      stiff(1,3,1) = mod * ( x + x * y) / z
      stiff(1,3,2) = mod * (- x**4 - 2 * x**3 * y**2 - 6 * x**3 * y
     +              - x * y**3 - 4 * x**3 - x**2 * y - 2 * x * y**2
     +              + x**2 + y + 2 * x +  x * y) / z
      stiff(1,3,3) = mod *(- 3 * x**3 - 5 * x**3 * y - 2 * x**3 * y**2
     +              - x * y**3 - 2 * x**2 * y - x * y**2
     +              - 2 * x**2 - y**2 + 2 * x * y +  x + 1) / z
      stiff(1,4,4) = G23

c  Assume all cracks stiffness tensor components to be small numbers
      do 20 i3 = 2, num
       do 25 i4 = 1, 6
        do 30 i5 = 1, 6
         stiff(i3,i4,i5) = 0.1
30      continue
25     continue
20    continue

      write(25,*) 'Stiffness tensors'
      do 35 ii3 = 1, num
       write(25,*)'Stiffness tensor #',ii3
       do 37 ii4 = 1, 6
        write(25,*) stiff(ii3,ii4,1),'   ',stiff(ii3,ii4,2),'   ',
     +              stiff(ii3,ii4,3),'   ',stiff(ii3,ii4,4),'   ',
     +              stiff(ii3,ii4,5),'   ',stiff(ii3,ii4,6)
37     continue
35    continue
c*************************************************************************
c     Eshelby Tensors
c*************************************************************************
      do 40 i7 = 1, num
       do 42 i8 = 1, 6
        do 45 i9 = 1, 6
         eshlby(i7,i8,i9) = 0.0
45      continue
42     continue
40    continue

      do 50 i6 = 2, num
      eshlby(i6,1,1) = 3.14159 * (13 - 8 * v32) * a3(num) /
```

```
     +              (32 * (1 - v32) * a2(num))
        eshlby(i6,2,2) = eshlby(i6,1,1)
          eshlby(i6,3,3) = 1 - (3.14159 * (1 - 2 * v32) * a3(num)) /
     +              (4 * (1 - v32) * a2(num))
        eshlby(i6,1,2) = 3.14159 * (8 * v32 - 1) * a3(num) /
     +              (32 * (1 - v32) * a2(num))
        eshlby(i6,2,1) = eshlby(i6,1,2)
          eshlby(i6,1,3) = (3.14159 * (2 * v32 - 1) * a3(num)) /
     +              (8 * (1 - v32) * a2(num))
        eshlby(i6,2,3) = eshlby(i6,1,3)
          eshlby(i6,3,1) = v32 / (1 - v32) *
     +              (1 - (3.14159 * (1 + 4 * v32) * a3(num))
     +                  / (8 * v32 * a2(num)))
        eshlby(i6,3,2) = eshlby(i6,3,1)
          eshlby(i6,6,6) = 3.14159 * (7 - 8 * v32) * a3(num) /
     +              (32 * (1 - v32) * a2(num))
        eshlby(i6,5,5) = (0.5) * (1 + (3.14159 * (v32 - 2) * a3(num)) /
     +              (4 * (1 - v32) * a2(num)))
          eshlby(i6,4,4) = eshlby(i6,5,5)

50      continue
        write(26,*) 'Eshelby tensors'
        do 55 ii6 = 1, num
          write(26,*)'Eshelby tensor #',ii6
          do 57 ii7 = 1, 6
            write(26,*) eshlby(ii6,ii7,1),'  ',eshlby(ii6,ii7,2),'  ',
     +                  eshlby(ii6,ii7,3),'  ',eshlby(ii6,ii7,4),'  ',
     +                  eshlby(ii6,ii7,5),'  ',eshlby(ii6,ii7,6)
57        continue
55      continue
c*************************************************************************
c       Solve eave22, eave33 (33-loading direction)
c*************************************************************************
        const1(1) = 0.0
        const1(2) = 0.0
        const2(1) = 0.0
        const2(2) = 0.0
        const3(1) = 0.0
        const3(2) = 0.0
        modtem = 0.0

        do 100 j = 2, num
          temp1(1,j) = stiff(1,2,1) * eshlby(j,1,2) * cos(theta(j))**2
     +              + stiff(1,2,1) * eshlby(j,1,3) * sin(theta(j))**2
     +              + stiff(1,2,2) * eshlby(j,2,2) * cos(theta(j))**2
     +              + stiff(1,2,2) * eshlby(j,2,3) * sin(theta(j))**2
     +              - stiff(1,2,2) * cos(theta(j))**2
     +              + stiff(1,2,3) * eshlby(j,3,2) * cos(theta(j))**2
     +              + stiff(1,2,3) * eshlby(j,3,3) * sin(theta(j))**2
     +              - stiff(1,2,3) * sin(theta(j))**2
          temp2(1,j) = -2 * stiff(1,2,1) * eshlby(j,1,2) * cos(theta(j))
     +     * sin(theta(j))
     +              + 2 * stiff(1,2,1) * eshlby(j,1,3) * sin(theta(j))
     +     * cos(theta(j))
```

```
+            - 2 * stiff(1,2,2) * eshlby(j,2,2) * cos(theta(j))
+     * sin(theta(j))
+            + 2 * stiff(1,2,2) * eshlby(j,2,3) * sin(theta(j))
+     * cos(theta(j))
+            + 2 * stiff(1,2,2) * sin(theta(j)) * cos(theta(j))
+            - 2 * stiff(1,2,3) * eshlby(j,3,2) * cos(theta(j))
+     * sin(theta(j))
+            + 2 * stiff(1,2,3) * eshlby(j,3,3) * sin(theta(j))
+     * cos(theta(j))
+            - 2 * stiff(1,2,3) * sin(theta(j)) * cos(theta(j))
      temp3(1,j) = stiff(1,2,1) * eshlby(j,1,2) * sin(theta(j))**2
+            + stiff(1,2,1) * eshlby(j,1,3) * cos(theta(j))**2
+            + stiff(1,2,2) * eshlby(j,2,2) * sin(theta(j))**2
+            + stiff(1,2,2) * eshlby(j,2,3) * cos(theta(j))**2
+            - stiff(1,2,2) * sin(theta(j))**2
+            + stiff(1,2,3) * eshlby(j,3,2) * sin(theta(j))**2
+            + stiff(1,2,3) * eshlby(j,3,3) * cos(theta(j))**2
+            - stiff(1,2,3) * cos(theta(j))**2

      temp1(2,j) = stiff(1,3,1) * eshlby(j,1,2) * cos(theta(j))**2
+            + stiff(1,3,1) * eshlby(j,1,3) * sin(theta(j))**2
+            + stiff(1,3,2) * eshlby(j,2,2) * cos(theta(j))**2
+            + stiff(1,3,2) * eshlby(j,2,3) * sin(theta(j))**2
+            - stiff(1,3,2) * cos(theta(j))**2
+            + stiff(1,3,3) * eshlby(j,3,2) * cos(theta(j))**2
+            + stiff(1,3,3) * eshlby(j,3,3) * sin(theta(j))**2
+            - stiff(1,3,3) * sin(theta(j))**2
      temp2(2,j) = -2 * stiff(1,3,1) * eshlby(j,1,2) * cos(theta(j))
+     * sin(theta(j))
+            + 2 * stiff(1,3,1) * eshlby(j,1,3) * sin(theta(j))
+     * cos(theta(j))
+            - 2 * stiff(1,3,2) * eshlby(j,2,2) * cos(theta(j))
+     * sin(theta(j))
+            + 2 * stiff(1,3,2) * eshlby(j,2,3) * sin(theta(j))
+     * cos(theta(j))
+            + 2 * stiff(1,3,2) * sin(theta(j)) * cos(theta(j))
+            - 2 * stiff(1,3,3) * eshlby(j,3,2) * cos(theta(j))
+     * sin(theta(j))
+            + 2 * stiff(1,3,3) * eshlby(j,3,3) * sin(theta(j))
+     * cos(theta(j))
+            - 2 * stiff(1,3,3) * sin(theta(j)) * cos(theta(j))
      temp3(2,j) = stiff(1,3,1) * eshlby(j,1,2) * sin(theta(j))**2
+            + stiff(1,3,1) * eshlby(j,1,3) * cos(theta(j))**2
+            + stiff(1,3,2) * eshlby(j,2,2) * sin(theta(j))**2
+            + stiff(1,3,2) * eshlby(j,2,3) * cos(theta(j))**2
+            - stiff(1,3,2) * sin(theta(j))**2
+            + stiff(1,3,3) * eshlby(j,3,2) * sin(theta(j))**2
+            + stiff(1,3,3) * eshlby(j,3,3) * cos(theta(j))**2
+            - stiff(1,3,3) * cos(theta(j))**2

      tempa(j) = stiff(1,2,1) * eshlby(j,1,2)
+            + stiff(1,2,2) * eshlby(j,2,2)
+            + stiff(1,2,3) * eshlby(j,3,2)
+            - stiff(1,2,2)
```

```
+               - stiff(j,2,2)
      tempb(j) = stiff(1,2,1) * eshlby(j,1,3)
+               + stiff(1,2,2) * eshlby(j,2,3)
+               + stiff(1,2,3) * eshlby(j,3,3)
+               - stiff(1,2,3)
+               - stiff(j,2,3)
      tempc(j) = stiff(j,2,2) - stiff(1,2,2)
      tempd(j) = stiff(j,2,3) - stiff(1,2,3)
      tempe(j) = stiff(1,3,1) * eshlby(j,1,2)
+               + stiff(1,3,2) * eshlby(j,2,2)
+               + stiff(1,3,3) * eshlby(j,3,2)
+               - stiff(1,3,2)
+               - stiff(j,3,2)
      tempf(j) = stiff(1,3,1) * eshlby(j,1,3)
+               + stiff(1,3,2) * eshlby(j,2,3)
+               + stiff(1,3,3) * eshlby(j,3,3)
+               - stiff(1,3,3)
+               - stiff(j,3,3)
      tempg(j) = stiff(j,3,2) - stiff(1,3,2)
      temph(j) = stiff(j,3,3) - stiff(1,3,3)

      tempr(j) = (tempf(j) * tempa(j) * tempc(j)
+          - tempa(j) * tempb(j) * tempg(j))
+          / (tempf(j) * tempa(j)**2
+               - tempe(j) * tempa(j) * tempb(j))
   temps(j) = (tempf(j) * tempa(j) * tempd(j)
+          - tempa(j) * tempb(j) * temph(j))
+          / (tempf(j) * tempa(j)**2
+               - tempe(j) * tempa(j) * tempb(j))
      tempt(j) = (tempa(j) * tempg(j) - tempe(j) * tempc(j))
+          / (tempf(j) * tempa(j) - tempe(j) * tempb(j))
      tempu(j) = (tempa(j) * temph(j) - tempd(j) * tempe(j))
+          / (tempf(j) * tempa(j) - tempe(j) * tempb(j))
   tempv(j) = (stiff(j,4,4) - stiff(1,4,4))
+          / (stiff(1,4,4) * eshlby(j,4,4)
+               + stiff(1,4,4)
+               - stiff(j,4,4))

      tempx1(j) = temps(j) * sin(theta(j))**2
+          + tempr(j) * cos(theta(j))**2
      tempx2(j) = tempr(j) * sin(theta(j))**2
+          + temps(j) * cos(theta(j))**2
   tempx3(j) = (tempr(j) * sin(theta(j))**2
+          - tempr(j) * v32 * cos(theta(j))**2
+          - temps(j) * v32 * sin(theta(j))**2
+          + temps(j) * cos(theta(j))**2)/mod

      tempy1(j) = -tempv(j) * sin(theta(j)) * cos(theta(j))
      tempy2(j) = tempv(j) * sin(theta(j)) * cos(theta(j))
   tempy3(j) = (tempv(j) * sin(theta(j)) * cos(theta(j))
+          + tempv(j) * v32 * cos(theta(j)) * sin(theta(j)))/mod

      tempz1(j) = tempu(j) * sin(theta(j))**2
+          + tempt(j) * cos(theta(j))**2
```

```
      tempz2(j) = tempt(j) * sin(theta(j))**2
     +          + tempu(j) * cos(theta(j))**2
     tempz3(j) = (tempt(j) * sin(theta(j))**2
     +          - tempt(j) * v32 * cos(theta(j))**2
     +          - tempu(j) * v32 * sin(theta(j))**2
     +          + tempu(j) * cos(theta(j))**2) / mod

      const1(1) = const1(1) + vf(j) * (temp1(1,j) * tempx1(j)
     +          + temp2(1,j) * tempy1(j) + temp3(1,j) * tempz1(j))
      const2(1) = const2(1) + vf(j) * (temp1(1,j) * tempx2(j)
     +          + temp2(1,j) * tempy2(j) + temp3(1,j) * tempz2(j))
     const3(1) = const3(1) + vf(j) * (temp1(1,j) * tempx3(j)
     +          + temp2(1,j) * tempy3(j) + temp3(1,j) * tempz3(j))

     const1(2) = const1(2) + vf(j) * (temp1(2,j) * tempx1(j)
     +          + temp2(2,j) * tempy1(j) + temp3(2,j) * tempz1(j))
      const2(2) = const2(2) + vf(j) * (temp1(2,j) * tempx2(j)
     +          + temp2(2,j) * tempy2(j) + temp3(2,j) * tempz2(j))
     const3(2) = const3(2) + vf(j) * (temp1(2,j) * tempx3(j)
     +          + temp2(2,j) * tempy3(j) + temp3(2,j) * tempz3(j))
       write(27,*) 'theta = ', theta(j) / 3.14159 * 180
       write(27,*) '*******************************'
       write(27,*) temp1(1,j),temp2(1,j),temp3(1,j)
       write(27,*) temp1(2,j),temp2(2,j),temp3(2,j)
       write(27,*) '--------------------------'
       write(27,*) tempa(j),tempb(j),tempc(j),tempd(j)
       write(27,*) tempe(j),tempf(j),tempg(j),temph(j)
       write(27,*) tempr(j),temps(j),tempt(j),tempu(j),tempv(j)
       write(27,*) '--------------------------'
       write(27,*) tempx1(j),tempx2(j),tempx3(j)
       write(27,*) tempy1(j),tempy2(j),tempy3(j)
       write(27,*) tempz1(j),tempz2(j),tempz3(j)
       write(27,*) '--------------------------'

100   continue

      const1(1) = const1(1) + stiff(1,2,2)
      const2(1) = const2(1) + stiff(1,2,3)
      const3(1) = -const3(1)
      const1(2) = const1(2) + stiff(1,3,2)
      const2(2) = const2(2) + stiff(1,3,3)
      const3(2) = -const3(2)

      write(27,*) const1(1),const2(1),const3(1)
      write(27,*) const1(2),const2(2),const3(2)

      test = const1(1) / const1(2)
      test1= const3(1) / const3(2)
      if (test .eq. test1) then
       eave22 = const3(1) / (const1(1) + const2(1))
       eave33 = eave22
        write(27,*) 'eave22 .eq. eave33'
      else
       test2 = const1(1) * const2(2) - const2(1) * const1(2)
```

```
          eave22=(const3(1) * const2(2) - const2(1) * const3(2)) / test2
          eave22=eave22/10.0
          eave33=(const1(1) * const3(2) - const1(2) * const3(1)) / test2
          write(27,*) 'eave22 .ne. eave33'
        endif
        write(27,*) 'eave22 = ',eave22,'     eave33 = ',eave33
c*************************************************************************
c       Calculating eastar3 of each volume fraction
c       Calculating Modulus of the composite
c*************************************************************************
        do 200 k = 2, num
          tempx(k) = tempx1(k) * eave22 + tempx2(k) * eave33 + tempx3(k)
          tempy(k) = tempy1(k) * eave22 + tempy2(k) * eave33 + tempy3(k)
          tempz(k) = tempz1(k) * eave22 + tempz2(k) * eave33 + tempz3(k)
          estar3(k) = sin(theta(k))**2 * tempx(k)
     +          + 2 * sin(theta(k)) * cos(theta(k)) * tempy(k)
     +               + cos(theta(k))**2 * tempz(k)
        write(27,*) '-------------------------'
          write(27,*) tempx(k),tempy(k),tempz(k)
          write(27,*) 'estar3 (',k,' ) = ',estar3(k)

          modtem = modtem + vf(k) * estar3(k)
200     continue
        modcom = mod / ( 1 + mod * modtem)
        write(27,*) 'Modulus of Composite = ', modcom,'  MPa'
        write(27,*) mod, modtem
        end
```